



Investigation of anti-cardiac hypertrophy effects of *Andrographis paniculata* ethanolic extract by modulating proinflammation and oxidative stress via Nrf2/NF-κB/NLRP3 signaling pathway: *In silico* and *in vitro* approaches

Muhamad Rizqy Fadhillah¹, Heri Wibowo², Arleni Bustami², Dewi Sukmawati³, Aryo Tedjo⁴, Nurul Gusti Khatimah¹, Ipppei Shimizu⁵, Wawaimuli Arozal^{6*}

¹Master Program in Biomedical Science, Faculty of Medicine, Universitas Indonesia, Jakarta, Indonesia.

²Integrated Laboratory, Faculty of Medicine, Universitas Indonesia, Jakarta, Indonesia.

³Department of Histology, Faculty of Medicine, Universitas Indonesia, Jakarta, Indonesia.

⁴Department of Medical Chemistry, Faculty of Medicine, Universitas Indonesia, Jakarta, Indonesia.

⁵Department of Cardiovascular Aging, National Cerebral and Cardiovascular Center, Osaka, Japan.

⁶Department of Pharmacology and Therapeutic, Faculty of Medicine, Universitas Indonesia, Jakarta, Indonesia.

ARTICLE HISTORY

Received on: 01/11/2024
Accepted on: 03/02/2025
Available Online: 05/05/2025

Key words:

Cardiac hypertrophy,
Andrographis paniculata,
Nrf2/NLRP3/NF-κB
signaling pathway, H9c2, *in silico* screening.

ABSTRACT

Previous studies showed that *Andrographis paniculata* exhibits antioxidant and anti-inflammatory properties, possibly by modulating the nuclear factor erythroid 2-related factor (Nrf2)/nuclear factor-kappa B (NF-κB)/NLR family pyrin domain-containing 3 (NLRP3) pathways. However, no research has investigated its potential for preventing cardiac hypertrophy through this pathway. This study aims to investigate the main compounds of *A. paniculata* ethanolic extract (APE) and decipher its potential effect against anti-cardiac hypertrophy by modulating Nrf2/NF-κB/NLRP3 pathways, using both *in vitro* and *in silico* approaches. APE metabolites were analyzed through qualitative reagent-based phytochemical testing and quantitative gas-chromatography mass-spectrometry (GC-MS) analysis. APE's anti-hypertrophic activity was evaluated in Ang-II-treated H9c2 cells. Cell-size area and hypertrophic gene expression were measured alongside proinflammatory mRNA expression (NF-κB, NLRP3, and IL-1β) and antioxidant mRNA expression (Nrf2, SOD1) with the levels of superoxide anion and hydrogen peroxide. The abundant compounds were analyzed using an *in silico* approach by docking, fingerprint analysis, and pharmacokinetic prediction. GC-MS showed that gamma-sitosterol, Andrographolide, Cortolone, stigmasterol, and 2,6,10,15,19,23-Pentamethyl-2,6,18,22-tetracosatetraen-10,15-diol were the most abundant in APE. *In vitro* studies showed APE suppresses Ang-II-treated H9c2 cell hypertrophy and limits the proinflammation and oxidative stress process through Nrf2/NF-κB/NLRP3 signaling. *In silico* studies revealed these compounds have low binding energy to Inhibitor of Kappa, Kelch-like ECH-associated protein 1, and NLRP3 proteins. They also exhibited good predicted IC₅₀ values, favorable ligand efficiency lipophilicity values, and a desirable pharmacokinetic profile. This *in vitro* study exhibited that APE inhibits the Ang-II-treated H9c2 hypertrophy by modulating proinflammation and oxidative stress through the Nrf2/Nf-κB/NLRP3 pathway, thereby reducing proinflammation and oxidative stress. *In silico* analysis found that the entire abundant compound exhibited good molecular interaction, with Andrographolide and Cortolone are potential drug candidates that need further investigation.

INTRODUCTION

Heart failure (HF) has emerged as a global concern, with a notable increase over the past three decades [1]. This rise is particularly pronounced in the Southeast Asian population, affecting approximately 10 million people in Indonesia [2].

*Corresponding Author
Wawaimuli Arozal, Department of Pharmacology and Therapeutic, Faculty of Medicine, Universitas Indonesia, Jakarta, Indonesia.
E-mail: wawaimuli.arozal@ui.ac.id

Currently, medications such as Angiotensin Receptor Blockers, Angiotensin-Converting Enzyme Inhibitors, Angiotensin Receptor-Nephrilysin Inhibitors, and Potassium-sparing diuretics are standard treatments for chronic HF patients [3]. Despite their efficacy, some patients could not tolerate their side effects—cough [4], hyperkalemia [5], angioedema [6], and renal insufficiency [7] and contraindication—pregnancy, renal stenosis, and HF with hypotension patients [7,8]. This fact emphasizes the need to explore alternative or complementary therapy, especially through natural resources.

A. paniculata, also called *sambiloto* or “King Bitter,” is a commonly found plant in Southeast Asia [9] and a prioritized medicinal plant that has become used as part of “jamu pahitan” in Indonesia [9,10]. This plant is rich in diterpenoid and flavonoid contents [11], which have many health effects [9] and are known to be safe [12]. Previous studies and some clinical trials [10,13–15] have revealed *sambiloto*’s efficacy, with antioxidant [16], anti-inflammatory [17], antimicrobial [18], antimalarial, anticancer [19], antiviral [20,21], and antidiabetic properties [10,22]. Some preclinical studies also proved that *A. paniculata* water extract inhibits the expression of key inflammatory markers such as cyclooxygenase-2, nuclear factor-kappa B (NF- κ B), phosphorylated inhibitor of kappa B, and interleukin-6 (IL-6) in the hearts of mice subjected to cardiac remodeling induced by a high-fat diet [23]. Additionally, in rat models of ischemia-reperfusion (I-R), hydroalcoholic extracts of *A. paniculata* improved cardiac dysfunction. They restored the expression of intrinsic antioxidant proteins [24]. Similar improvements in cardiac dysfunction also occurred in mongrel dogs subjected to I-R when water extract of *A. paniculata* [25].

Cardiac hypertrophy, an HF precursor, is typically triggered by risk factors associated with metabolic syndrome, such as hypertension, dyslipidemia, obesity, and diabetes mellitus [26–28]. These factors contribute to a gradual but persistent increase in oxidative stress and a proinflammatory state. The Renin-Angiotensin-Aldosterone System is a key pathway [29,30] for initiating pathological cardiomyocyte hypertrophy through oxidative stress [31] and inflammatory processes [32].

Regarding inflammation regulation, the NLR family pyrin domain-containing 3 (NLRP3) inflammasome has become a main target of therapy in pathological cardiac remodeling [33,34]. NLRP3 activation seems to be linked to the upregulation of NF- κ B [35] and the downregulation of nuclear factor erythroid 2-related factor (Nrf2). These are important transcription factors that crosstalk the expression of intrinsic antioxidants, anti-inflammatory and proinflammatory cytokines [36,37]. The Nrf2/NF- κ B/NLRP3 signaling pathway is a promising target in modulating cardiac hypertrophy by *A. paniculata*.

Our research group’s systematic review [38] found that *A. paniculata* and its bioactive compound, Andrographolide, have anticardiac hypertrophy properties, particularly by enhancing antioxidant activity and reducing the proinflammatory markers intracellularly. Andrographolide could upregulate Nrf2 myocardial infarction animal models [39]. Our previous research also showed the cardioprotective effect of dried *A. paniculata* ethanolic extract (APE) on doxorubicin-induced cardiotoxicity

rats by reducing the mRNA expression of NLRP3 and NF- κ B, further improving cardiac dysfunction [40,41]. Although APE reportedly has anti-inflammation and antioxidant effects, to the best of our knowledge, its potency in inhibiting hypertrophy of cardiomyocytes induced by angiotensin-II (Ang-II) through Nrf2/NLRP3/NF- κ B signaling has not yet been conducted. Based on current conditions, we aimed to investigate APE potency in mitigating cardiac hypertrophy progression using Ang-II treated H9c2 cells and capture its possibility of molecular interaction and potential candidates of the drug from bioactive compounds screened through *in silico* analysis.

MATERIAL AND METHODS

Material plants extraction procedure

APE was previously donated and formulated by PT Konimex (Sukaharjo, Indonesia) as a condensed paste extract. *A. paniculata* leaves from Semarang, Central Java, Indonesia, and a voucher specimen was deposited in the Faculty of Pharmacy, Universitas Gadjah Mada. Dried leaves were crushed into fine particles. Furthermore, dried plant material (1 kg) underwent percolation with 10 l of 90% ethanol, and the solvent was evaporated at 60°C under vacuum, as described in our previous study [40,41]. The formed condensed paste extract did not further dry using a fluid bed granulator, as explained in our in-press report. This condensed paste did not undergo Andrographolide profiling; thus, qualitative phytochemical screening, gas-chromatography mass-spectrometry (GC-MS) profiling, and total triterpenoid analysis were done.

Cells, chemical, and reagent

The H9c2 (2-1) rat cardiomyoblast (ATCC0, CRL-1446, CVCL-0286) cell line was provided by the Faculty of Medicine, Universitas Padjajaran, located in Bandung, West Java. Dulbecco’s modified Eagle medium (DMEM 1.0 g/l, L-glutamine, and sodium pyruvate, Cat. No. 10-014-CV), Fetal Bovine Serum (FBS, US Approved, Cat. No. 35-011-CV), and penicillin-streptomycin (Cat. No. 30-002-CI) were purchased from Corning® (Arizona, USA). Ang-II (Ang-II, HY-13948), 2’,7’-dichlorodihydrofluorescein (DCFH2-DA, Cat. No. HY-D0940), and dihydroethidium (DHE, HY-D0079) were obtained from Medchem Express (New Jersey, USA). Irbesartan was acquired from PT. Combiphar, Indonesia. Furthermore, 3-[4,5-dimethylthiazol-2-yl]-2,5 diphenyl tetrazolium bromide (MTT) (Vybrant® MTT Cell Proliferation Assay Kit, V-13154) and dimethyl sulfoxide (DMSO) were acquired from Thermo Fisher (Massachusetts, USA). Wright-Giemsa solutions (Cat. No. WG16) from Sigma-Aldrich® (Burlington, USA).

Qualitative phytochemical analysis

The extract’s qualitative profiling was initially conducted using reagents, followed by quantitative analysis using GC-MS. Qualitative phytochemical analysis was performed using Mayer, Dragendroff, Liebermann-Burchard, Braymer, Keller-Killiani, and Shinoda methods to identify various compounds, including alkaloids, steroids, terpenoids, saponins, flavonoids, and tannins, respectively.

Terpenoid total analysis

A. paniculata are known to be rich in diterpenoid content, especially Andrographolide. Terpenoid total analysis assesses the total terpenoid concentration contained in this extract. The procedure is performed in triplicate using a colorimetric-based assay with an ultraviolet Spectrophotometer at 551 nm and presented as mg/g of extract mass. APE's optical density (OD) will be compared with ursolic acid as a standard concentration.

Quantitative phytochemical analysis: GC-MS

This GC-MS is performed using untargeted metabolomic attempts to analyze all detectable compounds, including unknown ones [42]. Subsequently, the APE was subjected to (GC-MS, Shimadzu GC-MS-QP2020) to analyze the phytoconstituents present in the extract. The sample was prepared by the analysis using a direct capillary column SH-Rxi-5Sil MS with dimensions of 30 m × 0.25 mm × 0.25 m thickness. The column oven temperature was initially set at 50°C for 5 minutes, followed by a temperature ramp of 5°C/minute up to 280°C, which was maintained for 20 minutes. The injector and MS transfer lines were held at 280°C and 250°C, respectively. Helium was the carrier gas with a 1 ml/minute column flow rate. The solvent cut time was set at 2 minutes, and the diluted samples were injected using Shimadzu's AOC-20i/s Autosampler. Along with sample preparation using the autosampler, the sample was filtered and diluted the sample beforehand to test the dynamic range and instrument's sensitivity results. Shimadzu Electron Ionization mass spectra were collected in scan mode within the m/z 33–600 range. Identified compounds were compared with NIST17 mass spectral databases using retention time (RT) and mass spectra. The results obtained from GC-MS analysis included RT, % area, and similarity index (SI). The RT is defined as the time taken for the compound to travel through the GC column from injection to the detector measured in one minute. SI represents the quantification aspect of how close the mass spectrum detected in the unknown extract to the mass spectral database, whereas %area determined how much the concentration of specific detected in the test. APE solvent becomes an internal standard to calibrate and ensure the results validity of GC-MS testing.

Cell culture

H9c2 cells are ventricular embryonic rat BDIX cardiomyoblasts frequently used in cardiac hypertrophy studies models [43–45], showing similar responses to primary neonatal cardiomyocytes [46]. As stated in our previous study [47], the H9c2 cells were cultured in DMEM (Cat. No. 11885084) supplemented with 10% FBS (Cat. No. 10438026 and 1% penicillin-streptomycin solution. The cells were maintained at 37°C in a humidified atmosphere containing 5% CO₂. Culturing was performed in T25 flasks for 7 days, with media changed every 3 days. Passaging was conducted when the cells reached 70%–80% confluency.

Cell viability and toxicity assay

The cell viability assay was conducted using the MTT method, with a seeding density of 5,000 cells per well. The viability of H9c2 cells was assessed indirectly by evaluating

their metabolic activity, which involves converting MTT to formazan crystals within the mitochondria. The assay aimed to determine the optimal and safest dosage of APE for use in the treatment.

H9c2 cells were treated with various concentrations of APE ranging from 3.9 to 125 µg/ml for 48 hours and compared with a group without APE to assess cell viability. Following treatment, the cells were rinsed with phosphate-buffered saline (PBS) and incubated with MTT reagent according to the manufacturer's instructions. Subsequently, the formazan crystals' OD was measured using a microplate reader at an absorbance of 570 Å after being dissolved with DMSO for 10 minutes of incubation.

The APE toxicity profile was evaluated by determining its half-maximal inhibitory concentration (IC₅₀) and comparing it with doxorubicin (negative control) and Irbesartan (positive control). The results were then categorized using established criteria to assess APE safety and efficacy for potential therapeutic use [48]. APE's OD was transformed into IC₅₀ and calculated using the following formula:

$$IC_{50} \text{ of APE} = \frac{\text{OD of group without APE} - \text{OP with APE in specific dosage}}{\text{OP of group without APE}}$$

Hypertrophy induction experiment

For experimental procedures, the cells were seeded into various types of culture plates: a 96-well plate for cell viability assays and cell-size area (CSA) determination, a six-well plate for mRNA analysis, and a 12-well plate for oxidative stress assays. Before induction, the cells underwent serum starvation for 24 hours.

Subsequently, the cells were divided into four experimental groups for treatment purposes: control group (Con), negative control group treated with Ang-II, positive control group treated with Irbesartan (Irbe), and experimental group treated with APE.

Cell-size area determination

CSA, a commonly used parameter in many previous studies, calculates the 2D area of the cell interface to investigate hypertrophy. Wright-Giemsa staining was employed to obtain clear cell images and accurate calculations. This routine staining method uses methylene blue and eosin to stain the nucleus and cytoplasmic contents of cells. The methods we conducted are modified from previous research using hematoxylin-eosin staining [49] and Giemsa staining [50].

After the cells were treated with Ang-II, with or without Irbesartan or APE, in 96-well plates, they were washed twice with ice-cold PBS. Subsequently, 100% ice-cold methanol was added to each well and allowed to air-dry. The cells were then stained with methylene blue for 30 minutes and washed with distilled water. Eosin staining was performed for another 30 minutes, followed by washing with distilled water. The stained cells were observed under an inverted microscope, and their CSAs were measured in five different regions in each

group. A total of 150 cells, using five random 20× objective lens fields in each group, were calculated for their CSA using ImageJ® software by three blinded independent observers who conducted the measurements.

Oxidative stress parameters: DCFH2-DA and DHE assay

The DCFH2-DA and DHE are fluorescent probes that are routinely used to detect the generation of superoxide anions and hydrogen peroxide through microplate-based methods. A total of 20,000 cells per well in a 6-well plate for each group were trypsinized and washed with PBS three times. After centrifugation, the cells were incubated with DCFH2-DA at 5 μM and DHE at 10 μM for 30 minutes at 37°C. Subsequently, the cells were washed again with PBS three times.

Following the incubation period, the OD in the fluorometry was measured at excitation/emission wavelengths of 492/517 nm for DCFH2-DA and 518/616 nm for DHE, respectively. The OD readings were then converted into fold changes of fluorescence intensity, normalized with the blank OD readings, and compared with those of the control group.

Quantitative real-time polymerase chain reaction

A total of 1×10^6 cultured cells per well for each group were subjected to total RNA extraction using the Direct Zol RNA MiniPrep Plus kit with TRI reagent (Zymo Research, USA, R2053). Subsequently, 500 μg of extracted RNA was reverse transcribed using the ReverTra Ace qPCR RT Master Mix (Toyobo BioTech, Japan, FSQ-301) according to the manufacturer's instructions.

The relative gene expression levels of brain natriuretic peptide (BNP), AT1R, NLRP3, NF-κB, interleukin-1β (IL1B), Nrf2, and superoxide dismutase 1 (SOD1) were determined using reverse transcription-quantitative polymerase chain reaction (RT-qPCR) with an SYBR Green PCR kit (Toyobo BioTech, Japan, QPS201). β-actin was used as a housekeeping gene for normalization. The fold-change expression of each gene was quantified using Livak's method. Table 1 lists the primers used for RT-qPCR.

Molecular docking analysis

Molecular docking was done using Molegro Virtual Docker (MVD, Molexus, Odder, Denmark) [51]. Docking was initiated to confirm the interaction between the detected metabolite, especially the most abundant one to Kelch-like ECH-associated protein 1 (Keap1) (a regulator protein of Nrf2), the ATP-binding domain within NLRP3 domain, and the inhibitor of kappa B kinase (IKK kinase) (a regulator protein of NF-κB). Before initiating the docking process, we will download the 3D structures of each ligand in.sdf format from the PubChem Website (<https://pubchem.ncbi.nlm.nih.gov/>). Additionally, receptor files for Keap1 (PDB ID: 4I7B), NLRP3 (PDB ID: 7ALV), and IKK kinase (PDB ID: 4KIK) will come from the RCSB website (<https://www.rcsb.org/>). Following optimization of the receptor structures, the native ligands will be re-docked to their respective positions, ensuring the validity of the docking process with a root mean square deviation (RMSD) threshold of less than 2 Å.

Table 1. List of primer.

| Gene of interest | Primer Sequences |
|------------------|---|
| Beta-actin | F: 5'- TGT TGT CCC TGT ATG CCT CT -3' R: TAA TGT CAC GCA CGA TTT CC |
| BNP | F: 5'-TGG GCA GAA GAT AGA CCG GA-3' R: 5'-ACA ACC TCA GCC CGT CAC AG-3' |
| NLRP3 | F: 5'-CAG GAT CTC GCA TTG GTT CT-3' R: 5'-ACA ACC TCA GCC CGT CAC AG-3' |
| IL1B | F: 5'-CTG AAA GCT CTC CAC CTC AAT-3' R: 5'- CGT TGC TTG TCT CTC CTT CTA -3' |
| NFKB1 | F: 5'- TCA CAG ACA GAG AGA AGG AGA-3' R: 5'- AGG AAG GCT GTG AAC ATG GAG-3' |
| SOD1 | F: 5'- GGT CCA CGA GAA ACA AGA TGA-3' R: 5'- CAA TCC CAA TCA CAC CAC AAG -3' |
| NRF2 | F: 5'- CAT TGA GGG CTG TGA TCT GT-3' R: 5'- GGA CTT GTG TTC AGC GAA ATG-3' |
| AT1R | F: 5'- TGT CAT GAT CCC TAC CCT CTA C-3' R: 5'- GCC ACA GTC TTC AGC TTC AT-3' |

AT1R = angiotensin receptor 1; BNP = brain natriuretic peptide; IL1B = interleukin-1β; NFKB1 = nuclear factor kappa B subunit 1; NLRP3 = NLR family pyrin domain-containing 3; NRF2 = nuclear factor erythroid-2 related factor 2; SOD1 = superoxide dismutase 1.

MVD employs both internal and external energy of bonds created by the ligand on the binding site. Each compound will be docked into the same binding coordinates, and their binding affinity will be evaluated using the MolDockScore (kJ/mol). A negative MolDockScore indicates a strong binding affinity of the ligand to the target protein, providing valuable insights into potential therapeutic interactions.

Chemoinformatic analysis: Molecular fingerprint using machine learning

MFP is part of chemoinformatics performed to predict bioactivity and lipophilicity metrics in specific compounds against protein targets using publicly available databases. This research uses data from Chemical European Molecular Biology Laboratory (ChEMBL) accessed through DataWarrior®. The IC50 and ligand efficiency lipophilicity (LELP) incorporate bioactivity with the compound's physiochemical feature. SkelSpheres are used as molecular descriptors.

First, the Keap1 inhibitor dataset (ChEMBL Q14145; Uniprot K7E49), NLRP3 NACHT domain inhibitor (ChEMBL Q96P20; Uniprot), and IKK kinase inhibitor (ChEMBL O14920; O15111; Q9Y6K9; Uniprot) compounds were initially prepared using the ChEMBL database, which manually curates bioactive chemical molecules. Data containing IC₅₀ values were extracted and separated. The clustering of compounds to determine testing and training data was performed using the SkelSpheres descriptor with a similarity score threshold of 0.9. The dataset was divided into representative and non-representative data. Representative data were designated for testing purposes, while non-representative data were allocated

for training purposes. For predictive model validation, the IC_{50} values were transformed into $\text{Log } IC_{50}$, and LELP was calculated as one important parameter in drug discovery, combining bioactivity with the physiochemical feature of the drug [52].

In the testing data, the $\text{Log } IC_{50}$ values were considered the actual $\text{Log } IC_{50}$ (a $\text{Log } IC_{50}$) or actual LELP (aLELP) values. In contrast, the values predicted by the predictive model/machine learning were considered the predicted $\text{Log } IC_{50}$ (p $\text{Log } IC_{50}$) or predicted LELP (pLELP) values. To validate the $\text{Log } IC_{50}$ and LELP prediction models, support vector regression (SVR) was employed for the data training. The models' performance was evaluated by measuring the R -square (R^2 , $R^2 > 0.5$) values and Pearson correlation coefficients (r) [53,54]. These metrics were calculated by comparing p $\text{Log } IC_{50}$ or pLELP and a $\text{Log } IC_{50}$ or pLELP values of the Keap1, IKK, and NLRP3 inhibitor compounds in the testing data. These steps are also done for the LELP parameter. After the system is validated, we input canonical the simplified molecular-input line-entry system of APE metabolites and then run the prediction through our built dataset. The IC_{50} of each compound will be categorized based on established criteria [48], whereas metabolites with ideal LELP are within the range -10 and $+10$ [52].

Table 2. Phytochemical screening results.

| Group compound | Name of Test | Results |
|----------------|-----------------------|---------|
| Saponin | Shaking | - |
| Tannin | Braymer's test | + |
| Flavonoid | Sinoda Test | + |
| Glycosides | Killer kiliani | - |
| Terpenoid | Liebermann-Burchard | + |
| Steroid | Liebermann-Burchard | + |
| Alkaloid | Mayer and Dragendroff | - |

Computational pharmacokinetic and toxicity analysis

Physicochemical properties influence drug candidates' administration, distribution, metabolism, excretion, and toxicities (ADMETs). In addition, drug-likeness (DL) prediction was performed using Lipinski's Rule of Five [55] which assesses molecular properties related to drug absorption and permeation. SwissADME (<https://swissadme.ch>) and pKCSM (<https://biosig.lab.uq.edu.au/pkcsml/prediction>) were employed to predict DL and ADMET variables, respectively, by inputting canonical smiles. Compounds that do not violate Lipinski's Rule of Five have undergone molecular docking and molecular fingerprint (MFP) analysis. For each detected compound, further toxicity predictions were made using Protox 3 (https://comptox.charite.de/protox3/index.php?site=compound_input).

Statistical analysis

All *in vitro* data collected were analyzed using GraphPad Prism 10 (GraphPad Software Inc.). Descriptive statistics were presented as mean \pm SEM. Bivariate analysis was performed using analysis of variance followed by Bonferroni analysis for multiple comparisons. Statistical significance was determined at a p -value threshold below 0.05. This statistical analysis was also done for the validation methods of MFP for predicting the IC_{50} and LELP parameters for the entire compound using R^2 and Spearman correlation the result will be provided in supplementary materials.

RESULTS

APE qualitative phytochemical, GC-MS, and terpenoid analysis

The qualitative phytochemical analysis identified tannin, flavonoid, terpenoid, and steroid using specific reagents in this extract (Table 2). The results were then confirmed through GC-MS (Fig. 1), and thirty metabolites were detected (Table 3). Among these thirty compounds, gamma-sitosterol

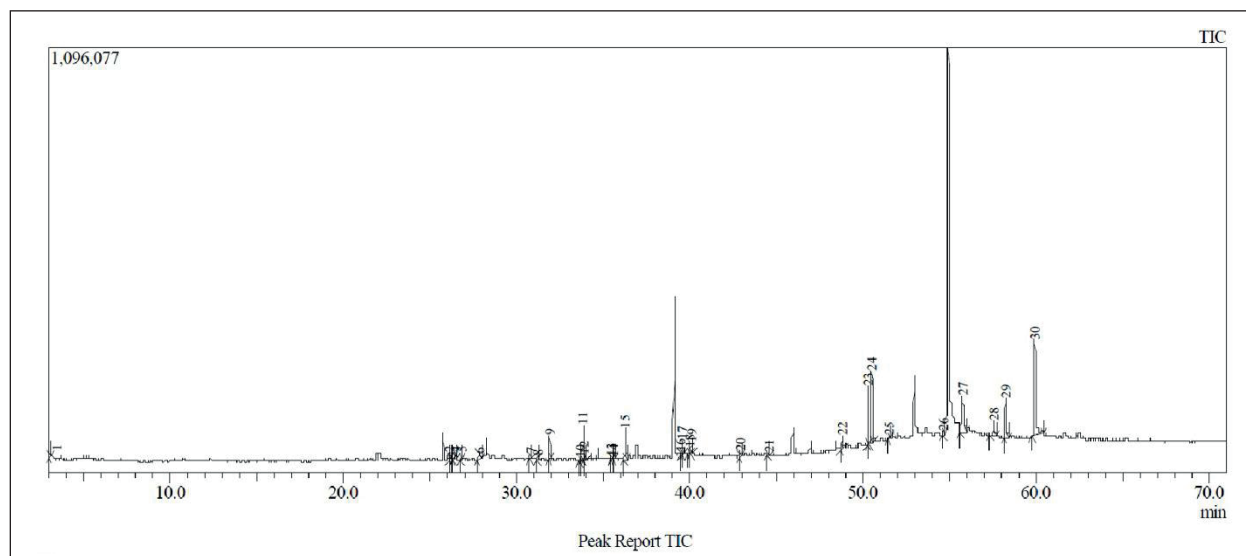


Figure 1. GC-MS analysis of *A. paniculata* ethanolic extract (APE).

(26.99%), Andrographolide (12.28%), Cortolone (11.0%), stigmasterol (10.05%), and 2,6,10,15,19,23-pentamethyl-2,6,18,22-tetracosatetraen-10,15-diol (PMT) (6.08%) become the most abundant metabolites in extract. Mass-spectral of each predominant compound present in the supplementary file. Our experiments identified the total terpenoid concentration in this extract reaching $52.1 \pm 0.2\%$ mg/mg.

Viability and cytotoxicity profile of APE in H9c2 cardiomyoblast

APE started to reduce the H9c2 viability even in the lowest tested dosage (3.9 $\mu\text{g/ml}$), as presented in Figure 2A. Using the exact APE dosage group, we tried adding Ang-II 1 μM to see the change in H9c2 viability (Fig. 2b). However, the changes are not different, and the reduction of viability was observed even in the lowest tested dosage of extract, with relatively similar IC_{50} (APE only vs. APE with Ang-II, 17.65 vs. 22.68 $\mu\text{g/ml}$), classified as strong cytotoxicity (10–100 $\mu\text{g/ml}$), based on established criteria [48] (Fig. 2c). The H9c2 viability is only reduced in the 2.5 μM (Fig. 2d) for Ang-II dosage determination. Regarding the cytotoxicity profile, doxorubicin has more cytotoxicity activity than APE, as demonstrated in this research, which reduces cell viability starting from 0.12 μM (Fig. 2e). Irbesartan 1 μM is the selected dosage for positive control based on a previous study and did not reduce cell viability (Fig. 2f) [56]. Based on our IC_{50} result above, we used approximately the lowest half of IC_{50} detected, becoming 9 $\mu\text{g/ml}$ concentration of APE as tested dosage to find APE antihypertrophic activity. In addition, this dosage showed a minimum reduction of H9c2 viability.

The effect of APE on CSA and mRNA expression BNP and angiotensin receptor 1 (AT1R)

The H9c2 exposed by Ang-II significantly demonstrated increasing CSA and upregulation of BNP and AT1R mRNA expression compared to the control group. The APE significantly reduced the CSA of Ang-II treated H9c2 compared to the Ang-II group, even though the reduction is not much like the Irbesartan group (Fig. 3a and b, see supplementary file). Furthermore, this finding is also supported by the decrease in the expression of BNP (Fig. 3c) and AT1R in the APE group (Fig. 3d).

The effect of APE in superoxide anion and hydrogen peroxide production on Ang-II-treated H9c2 cells

The Ang-II-treated H9c2 showed significantly increased intracellular superoxide anion and hydrogen peroxide production. Superoxide anion (Fig. 4a) and hydrogen peroxide (Fig. 4b) were markedly reduced after the cells were treated with APE ($p < 0.05$), even though for reactive oxygen species (ROS), the reduction was not as much as the Irbesartan group.

The effect of APE in the Nrf2 and SOD1 the mRNA expression

Following the Ang-II exposure, Nrf2 and SOD1 mRNA expression were significantly suppressed in Ang-II-treated H9c2 cells ($p < 0.05$). Furthermore, the APE reverted the mRNA expression of both genes significantly ($p < 0.05$), comparable to Irbesartan, which shows that the APE recovered the antioxidant defense mechanism (Fig. 4c and d).

Table 3. List of compound in AP ethanolic extract detected in GC-MS.

| Selected compound | SI | RT | %Area |
|---|----|--------|-------|
| Ethane, 1,1-diethoxy- | 88 | 3.051 | 0.5 |
| (-)-Zingiberene | 93 | 26.135 | 0.59 |
| Benzoic acid, 2-hydroxy-4-methoxy-6-methyl- | 84 | 26.317 | 0.05 |
| Beta curcumene | 87 | 26.5 | 1.02 |
| Sesquiphellandrene | 93 | 26.858 | 0.69 |
| Diethyl Phthalate | 91 | 27.892 | 1.69 |
| Germacron | 88 | 30.858 | 0.73 |
| Pentadecanal- | 80 | 31.252 | 0.36 |
| Xanthorrhizol | 91 | 31.947 | 2.67 |
| Neophytadiene | 95 | 33.841 | 3.72 |
| Phytyl acetate | 91 | 33.841 | 0.48 |
| Fitone | 85 | 33.925 | 1.47 |
| Eicosanal- | 80 | 35.509 | 0.17 |
| Hexadecanoic acid, ethyl ester | 94 | 35.617 | 0.28 |
| Palmitic acid | 93 | 36.286 | 5.34 |
| Phytol | 91 | 39.122 | 0.48 |
| 9,12-Octadecadien-1-ol, (Z,Z)- | 85 | 39.483 | 0.47 |
| 9,12,15-Octadecatrienoic acid, (Z,Z,Z)- | 91 | 39.595 | 2.50 |
| Linoleic acid ethyl ester | 86 | 40.025 | 0.81 |
| 9,12,15-Octadecatrienoic acid, ethyl ester, (Z,Z,Z)- | 88 | 40.133 | 1.33 |
| Henicosanal | 88 | 42.942 | 0.50 |
| Docosanal | 86 | 44.608 | 0.33 |
| 7-O-Methylwogonin | 91 | 48.853 | 2.88 |
| 2,6,10,15,19,23-Pentamethyl-2,6,18,22-tetracosatetraen-10,15-diol | 94 | 50.328 | 6.08 |
| Cortolone | 80 | 50.533 | 11.00 |
| Tetrapentacontane | 82 | 51.55 | 0.37 |
| Andrographolide | 81 | 55.8 | 12.28 |
| Campesterol | 81 | 57.608 | 3.94 |
| Stigmasterol | 83 | 58.283 | 10.05 |
| Gamma-Sitosterol | 85 | 59.967 | 26.99 |

%Area = percentage area of under curve; RT: retention time.

The effect of APE in the NF- κ B, NLRP3, and IL-1 β the mRNA expression

Ang-II exposure to H9c2 in this study showed upregulation of intracellular NF- κ B, NLRP3, and IL-1 β mRNA expression. Furthermore, the APE reverted the mRNA expression of NF- κ B (Fig. 5a), NLRP3 (Fig. 5b), and IL-1 β (Fig. 5c) in Ang-II-treated H9c2 significantly ($p < 0.05$) and comparable with Irbesartan showing that the APE activity in modulating the proinflammation signaling.

DL properties of secondary metabolites detected in APE

DL properties reflect characteristics of molecules that indicate their suitability to become safe and effective drugs. We used Lipinski's Rule of Five, which consists of the number of molecular weights no more than 500 Da, Hydrogen acceptor

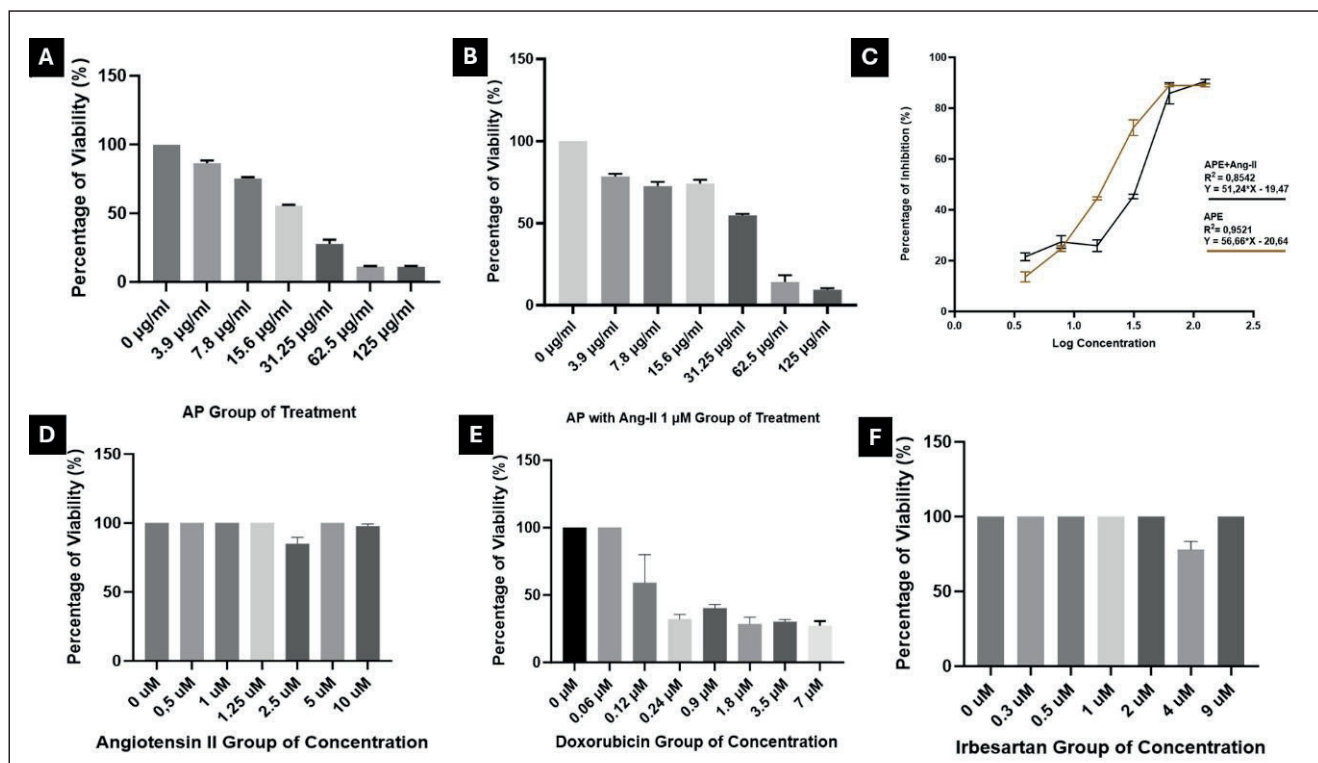


Figure 2. Viability and cytotoxicity testing of H9c2 cells, (A) viability test of APE, (B) viability test of APE with Ang-II 1 µM, (C) cytotoxicity testing of APE and APE with Ang-II 1 µM, (D) viability testing of Ang-II, (E) viability testing of doxorubicin, and (F) viability testing of doxorubicin. Ang-II: angiotensin-II. ($n = \text{triplicate}$); APE = *A. paniculata* ethanolic extract; $*p < 0.05$.

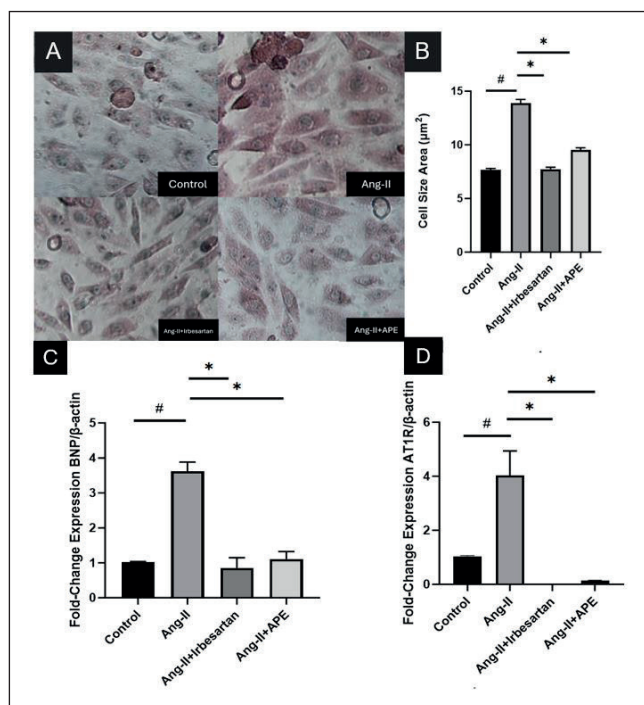


Figure 3. Hypertrophic testing results (A) Wright-Giemsa staining (B) cell-size area (C) BNP fold-change expression, and (D) AT1R fold-change expression; $\#p < 0.05$ versus Ang-II, $*p < 0.05$ versus Ang-II+Irbesartan, and Ang-II+APE. AT1R = angiotensin-II receptor 1; BNP = brain natriuretic peptide. ($n = \text{triplicate}$).

below 10, Hydrogen donor below 5, and CLogP less than 4.15 through SwissADME prediction and summarized the results for entire secondary metabolites in Table 4. Since 29 metabolites have good drug-like properties, except tetrapentacone, they will further continue molecular docking and fingerprint analysis.

Predominant metabolites in APE have negative energy binding to the Keap1, IKK, and NLRP3 in molecular docking

Before performing molecular docking, the protein quality is checked. We strictly use.pdb files with Resolution $< 3 \text{ \AA}$ and good Ramachandran criteria for each.pdb file. Since the selected.pdb files have their native ligands, the redocking methods were used to check the validity, which is proven by the RMSD $< 2 \text{ \AA}$ for Keap1 (Fig. 6a), IKK (Fig. 6b), and NLRP3 (Fig. 6c). As present in our *in vitro* model, Irbesartan could modulate mRNA expression of NF- κ B, NLRP3, and Nrf2. Hence, we also used Irbesartan as a standard drug in molecular docking and compared its MolDock and Rerank Score to the detected metabolites. The exact direction of the binding site of each protein is summarized in Table 5. Among the 30 compounds docked to Keap1, IKK, and NLRP3, PMT has the lowest MolDock and Rerank Score compared to other metabolites detected in GC-MS (see supplementary materials). Irbesartan shows low binding energy against IKK and NLRP3 as a positive control but not for Keap1. In this study, PMT showed much lower binding energy than the other molecules found in the APE. Furthermore, the entire metabolite showed a negative MolDock Score and Rerank Score, as well as the

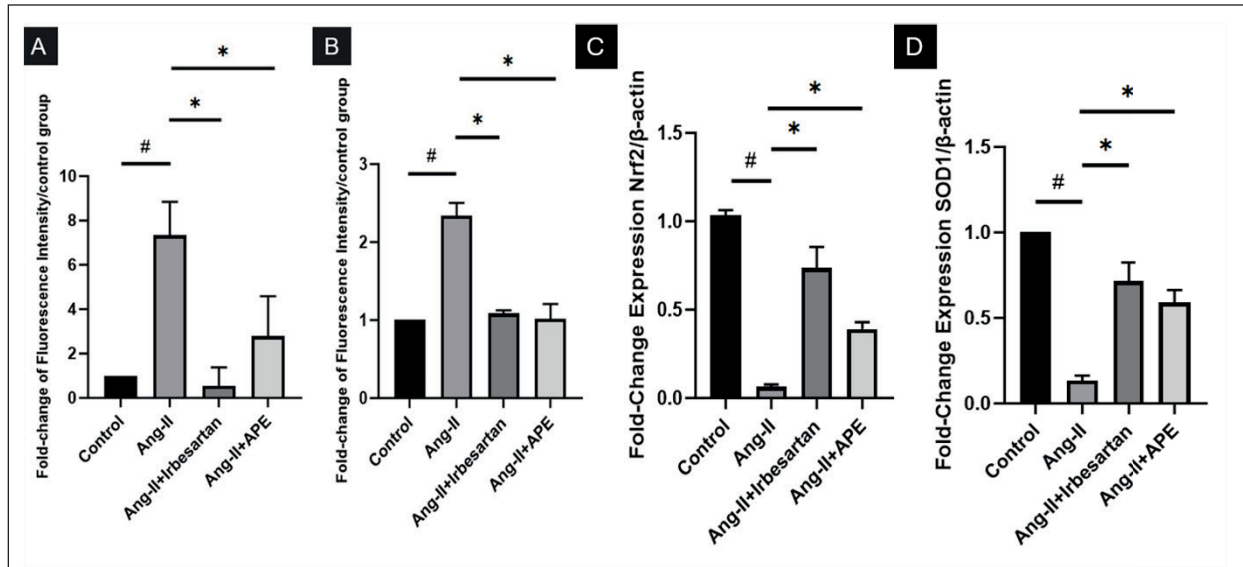


Figure 4. Oxidative stress parameters (a) relative superoxide anion level (DCFHDA), (b) relative hydrogen peroxide level (DHE), (c) Nrf2 mRNA fold-change expression, and (d) SOD1 mRNA fold-change expression; #*p* < 0.05 versus Ang-II, **p* < 0.05 versus Ang-II+Irbesartan, and Ang-II+APE. DCFH2-DA = 2',7'-dichlorodihydrofluorescein; DHE = dihydroethidium. (*n* = triplicate).

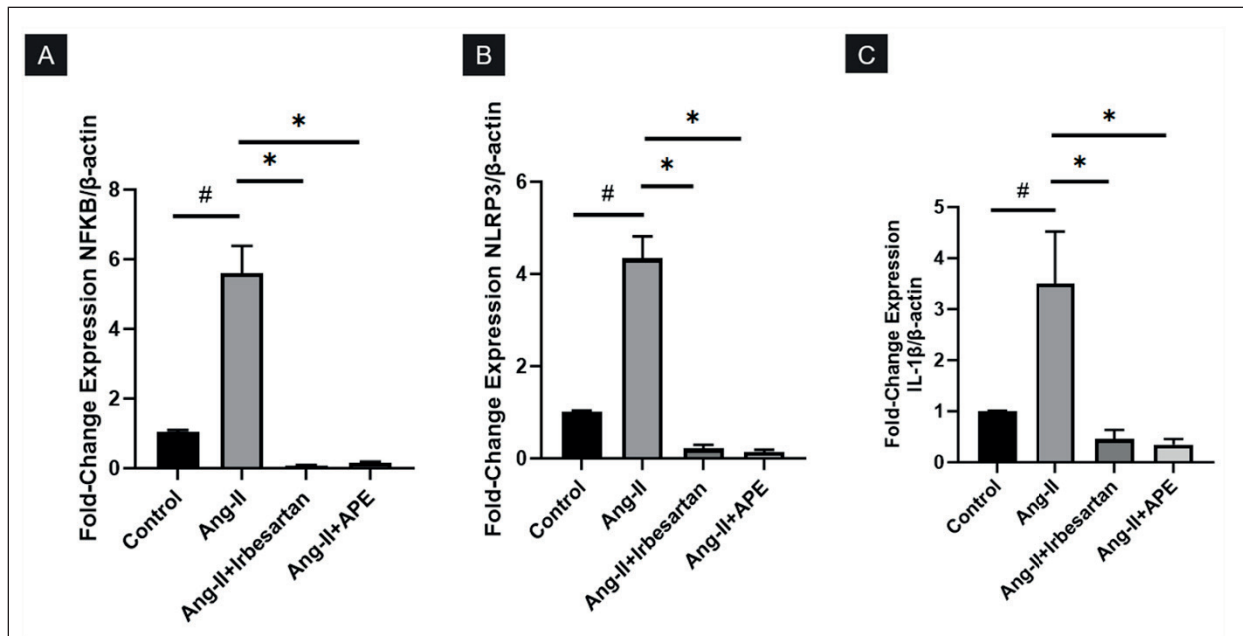


Figure 5. Proinflammation parameters, (a) Nf-κB mRNA fold-change expression, (b) NLRP3 mRNA fold-change expression, and (c) IL-1β mRNA fold-change expression; #*p* < 0.05 versus Ang-II, **p* < 0.05 versus Ang-II+Irbesartan, and Ang-II+APE. IL-1β = Interleukin-1β; Nf-κB = Nuclear Factor-Kappa B; NLRP3 = NLR family pyrin domain-containing 3. (*n* = triplicate).

five predominant metabolites to the Keap1, IKK, and NLRP3 that judge their spontaneous binding to the active site of the corresponding protein (Table 6).

As the lowest ligand to interact with Keap1, the hydrogen bond site created by PMT (Arg415 and Ser602) is different from Irbesartan (Asn387 and Ser555), but similar to the native ligand, but not for other predominant compounds. Stigmasterol had more hydrogen bonds than gamma-sitosterol, Andrographolide, and Cortolone. Furthermore, even Cortolone

has higher Moldock and Rerank scores than other predominant compounds. It interacts with binding sites through hydrogen bonds with almost similar amino acids with native ligands at Ser602 (Fig. 7).

Different interactions with IKK protein, even PMT having the lowest binding energy and the amino acid contributing to the hydrogen bond (Asp166, Lys44), are different from those of the native ligand. Cortolone has higher binding energy and more hydrogen bonds than other

Table 4. Druglikeness feature of entire metabolites.

| No | Molecular formula | Compound name | MW | H-bond acceptor | H-bond donor | MLogP | Lipinski's violation |
|----|-------------------|---|--------|-----------------|--------------|-------|----------------------|
| 1 | C6H14O2 | Ethane, 1,1-diethoxy- | 118.17 | 2 | 0 | 101 | 0 |
| 2 | C15H24 | (-)-Zingiberene | 204.35 | 0 | 0 | 453 | 1 |
| 3 | C9H10O4 | Benzoic acid, 2-hydroxy-4-methoxy-6-methyl- | 182.17 | 4 | 2 | 106 | 0 |
| 4 | C15H24 | Beta curcumene | 204.35 | 0 | 0 | 453 | 1 |
| 5 | C15H24 | Sesquiphellandrene | 204.35 | 0 | 0 | 453 | 1 |
| 6 | C12H14O4 | Diethyl Phthalate | 222.24 | 4 | 0 | 239 | 0 |
| 7 | C15H22O | Germacon | 218.33 | 1 | 0 | 337 | 0 |
| 8 | C15H30O | Pentadecanal- | 226.4 | 1 | 0 | 406 | 0 |
| 9 | C15H22O | Xanthorrhizol | 218.33 | 1 | 1 | 403 | 0 |
| 10 | C20H38 | Neophytadiene | 278.52 | 0 | 0 | 621 | 1 |
| 11 | C22H42O2 | Phytol acetate | 338.57 | 2 | 0 | 547 | 1 |
| 12 | C18H36O | Fitone | 268.48 | 1 | 0 | 479 | 1 |
| 13 | C20H40O | Eicosanal- | 296.53 | 1 | 0 | 525 | 1 |
| 14 | C18H36O2 | Hexadecanoic acid, ethyl ester | 284.48 | 2 | 0 | 467 | 1 |
| 15 | C16H32O2 | Palmitic acid | 256.42 | 2 | 1 | 419 | 1 |
| 16 | C20H40O | Phytol | 296.53 | 1 | 1 | 525 | 1 |
| 17 | C18H34O | 9,12-Octadecadien-1-ol, (Z,Z)- | 266.46 | 1 | 1 | 468 | 1 |
| 18 | C18H30O2 | 9,12,15-Octadecatrienoic acid, (Z,Z,Z)- | 278.43 | 2 | 1 | 438 | 1 |
| 19 | C20H36O2 | Linoleic acid ethyl ester | 308.5 | 2 | 0 | 493 | 1 |
| 20 | C20H34O2 | 9,12,15-Octadecatrienoic acid, ethyl ester, (Z,Z,Z)- | 306.48 | 2 | 0 | 484 | 1 |
| 21 | C21H42O | Henicosanal | 310.56 | 1 | 0 | 547 | 1 |
| 22 | C22H44O | Docosanal | 324.58 | 1 | 0 | 569 | 1 |
| 23 | C17H14O5 | 7-O-Methylwogonin | 298.29 | 5 | 1 | 101 | 0 |
| 24 | C30H54O2 | 2,6,10,15,19,23-Pentamethyl-2,6,18,22-tetracosatetraen-10,15-diol | 446.75 | 2 | 2 | 609 | 1 |
| 25 | C21H34O5 | Cortolone | 366.49 | 5 | 4 | 159 | 0 |
| 26 | C54H110 | Tetrapentacontane | 759.45 | 0 | 0 | 1,349 | 2 |
| 27 | C20H30O5 | Andrographolide | 350.45 | 5 | 3 | 198 | 0 |
| 28 | C28H48O | Campesterol | 400.68 | 1 | 1 | 654 | 1 |
| 29 | C29H48O | Stigmasterol | 412.69 | 1 | 1 | 662 | 1 |
| 30 | C29H50O | Gamma-Sitosterol | 414.71 | 1 | 1 | 673 | 1 |

predominant compounds through Glu97, Cys99, and Glu149 (Fig. 8).

PMT also showed lower binding energy with NLRP3 than Irbesartan (-161.702 kJ/mol) through hydrogen bonds formed through Arg578. Interestingly, Andrographolide formed hydrogen bonds with five amino acids in the NLRP3 active site (Ala228, Arg351, Pro352, Val353, and Asp662). In addition, Cortolone shows three hydrogen bonds through Thr439, Arg578, and Glu629 amino acids (Fig. 9).

Predominant metabolites in APE have good predicted bioactivity and LELP to the Keap1, IKK kinase, and NLRP3

The Keap1, IKK, and NLRP3 inhibitor data retrieved from DataWarrior® are 1721, 78, and 908 data, respectively.

After data cleansing, including omitting the non-IC50 and blank data, it resulted in 306, 59, and 527 compounds for Keap1, IKK, and NLRP3 inhibitors. The data then split based on the similarity (0.9) yielded 76, 15, and 241 representative compounds for each included protein. The non-representative data will be used as training. The data validation results were summarized in Figure 10 for each dataset of proteins. R^2 and Spearman correlation were employed to determine data validation and showed our SVR prediction that each Log IC50 and LELP dataset has R^2 above >0.5 and Spearman correlation >0.5, which shows good correlation and data linearity as described in a previous publication [53,54]. Details of each compound found in APE with their predicted IC₅₀ and LELP against Keap1, IKK, and NLRP3 are summarized in our electronic data supplementation.

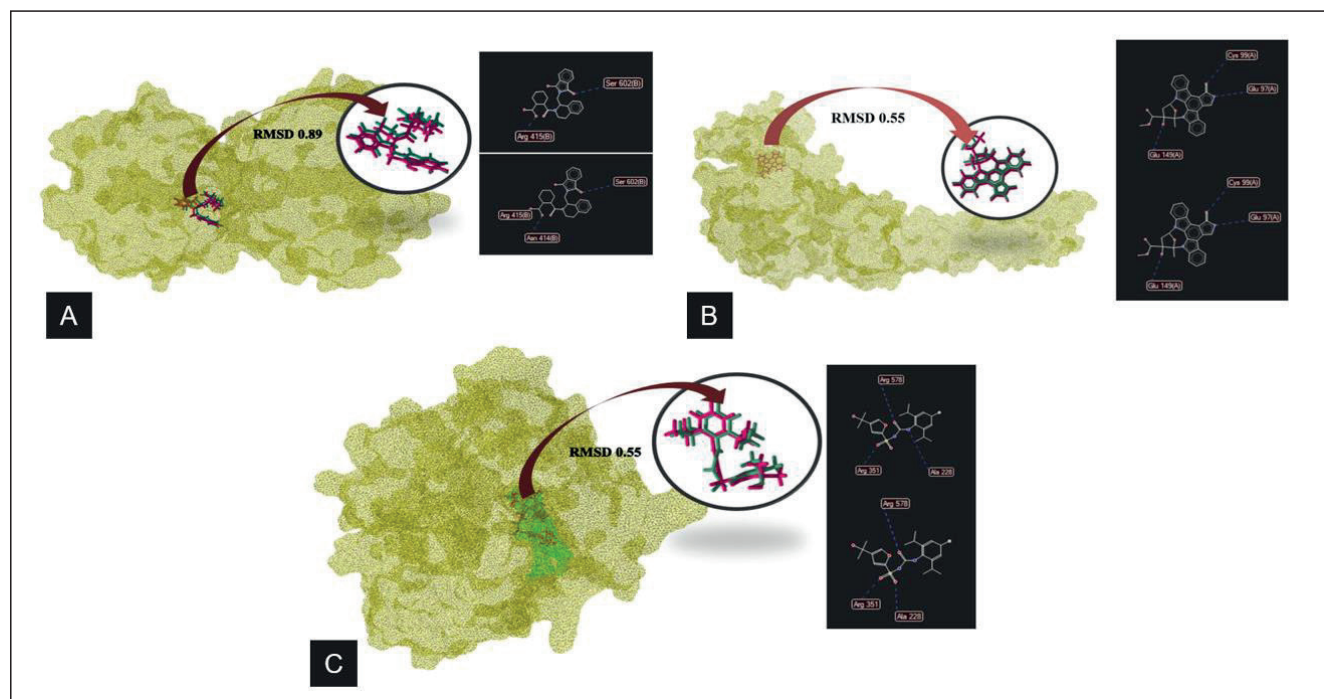


Figure 6. Validation of redocking in molecular docking (A) Keap1 redocking, (B) IKK redocking, and (C) NLRP3 redocking, which shows RMSD <math>< 2 \text{ \AA}</math>. IKK = inhibitor of Kappa B kinase; Keap1 = Kelch-like ECH associated protein 1; NLRP3 = NLR family pyrin domain-containing 3 (NLRP3) inflammasome; RMSD = root mean square deviation.

Table 5. Optimal binding site of Keap1, IKK Kinase, and NLRP3 protein.

| RSCB data | Radius | X-axis | Y-axis | Z-axis |
|--------------|--------|--------|--------|--------|
| Keap1 (4I7B) | 10 | -3.47 | 2.29 | -27.53 |
| IKK (4KIK) | 10 | -14.04 | -31.81 | -73.34 |
| NLRP3 (7ALV) | 10 | 17.03 | 35.46 | 125.55 |

Table 6. Molecular docking results of predominant compound to Keap1, IKK, and NLRP3.

| Compound | Protein of interest | | | | | | | | |
|------------------|---------------------|--------------|------------------------|---------------|--------------|----------------------|---------------|--------------|--|
| | Keap1 | | | IKK | | | NLRP3 | | |
| | MolDock score | Rerank score | H-bond amino acid | MolDock score | Rerank score | H-bond amino acid | MolDock score | Rerank score | H-bond amino acid |
| Gamma-sitosterol | -145.3 | -108.6 | Ser383 | -129.8 | -34.7 | Lys106 | -134.5 | -108.7 | Gln624, Ser626 |
| Andrographolide | -122.5 | -88.6 | Arg380, Asn382 | -119.6 | -94.7 | Asp103, Asp166 | -116.3 | -97.7 | Ala228, Arg351, Pro352, Val353, Asp662 |
| Cortolone | -101.6 | -88.9 | Ser555, Ser602 | -95.1 | -49.4 | Glu97, Cys99, Glu149 | -97.3 | -89.1 | Thr439, Arg578, Glu629 |
| Stigmasterol | -134.7 | -105.5 | Asn387, Asn382, Ser383 | -126.6 | -33.4 | N/A | -131.1 | -55.1 | Gln624, Ser626 |
| PMT | -168.3 | -114.1 | Arg415, Ser602 | -156.1 | -83.6 | Asp166, Lys44 | -161.7 | -100.5 | Arg578 |

PMT: 2,6,10,15,19,23-Pentamethyl-2,6,18,22-tetracosatetraen-10,15-diol.

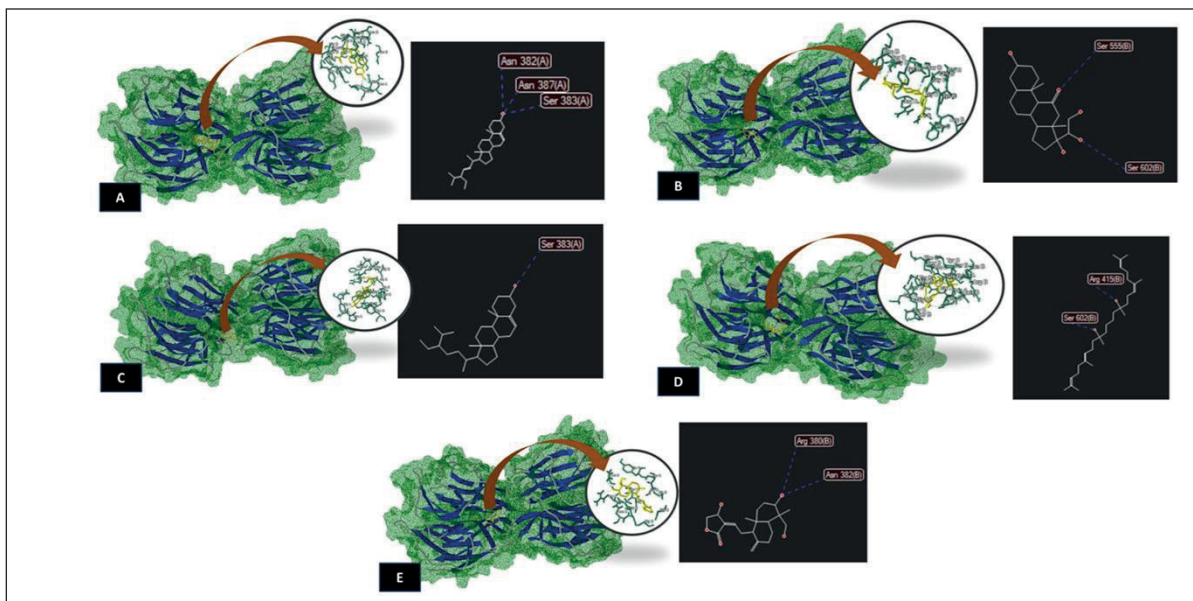


Figure 7. Two and three-dimensional visualization of the interaction of the five selected compounds to the Keap1 protein binding site (A) stigmasterol, (B) cortolone, (C) gamma-sitosterol, (D) PMT, and (E) andrographolide. Keap1 = Kelch-like ECH associated protein 1; PMT: 2,6,10,15,19,23-Pentamethyl-2,6,18,22-tetracosatetraen-10,15-diol.

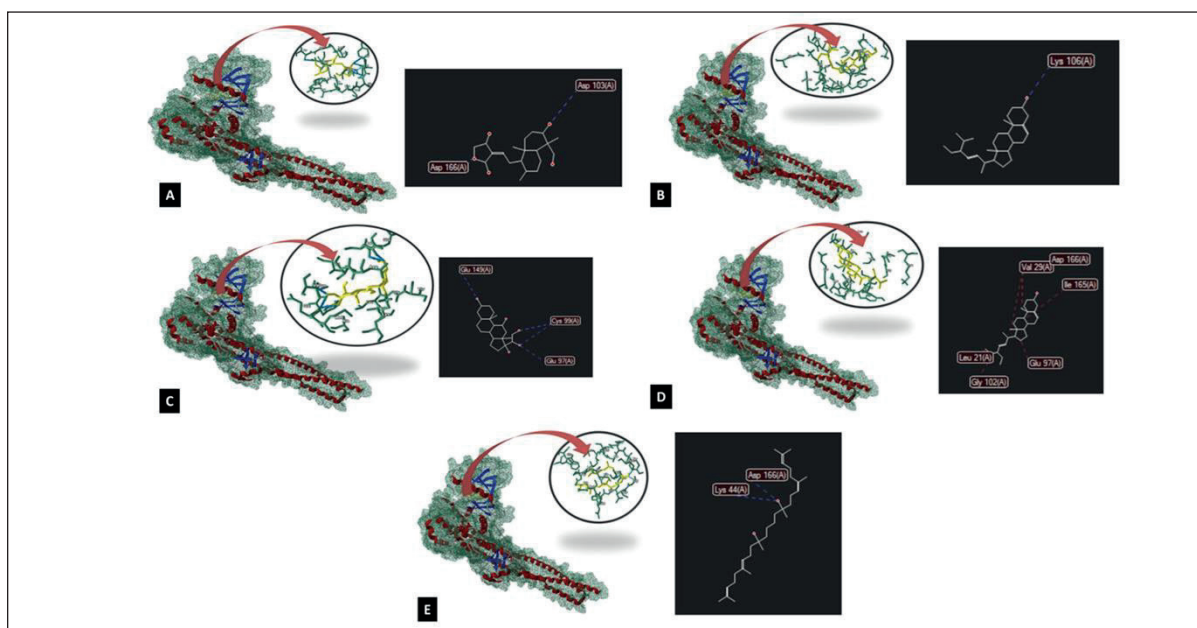


Figure 8. Two and three-dimensional visualization of the interaction of the five selected compounds to the IKK protein binding site (A) andrographolide, (B) gamma-sitosterol, (C) cortolone, (D) stigmasterol, and (E) PMT. IKK = inhibitor of Kappa B kinase; PMT: 2,6,10,15,19,23-Pentamethyl-2,6,18,22-tetracosatetraen-10,15-diol.

Based on the SkelSpheres descriptor of predominant detected compounds, the pIC₅₀ of each compound has good activity (1–20 μM), except PMT, which shows excellent activity (0.2 μM) against Keap1 protein. Despite having good bioactivity, only Andrographolide and Cortolone showed an ideal LELP value (below 10) against Keap1, IKK, and NLRP3 (Table 7).

Computational prediction of pharmacokinetics and toxicity of predominant compound

Table 8 summarizes the pharmacokinetic and toxicity profiles for all compounds. Andrographolide and Cortolone exhibit good oral absorption with low blood–brain barrier penetration. Regarding metabolism, PMT inhibits CYP1A2 and

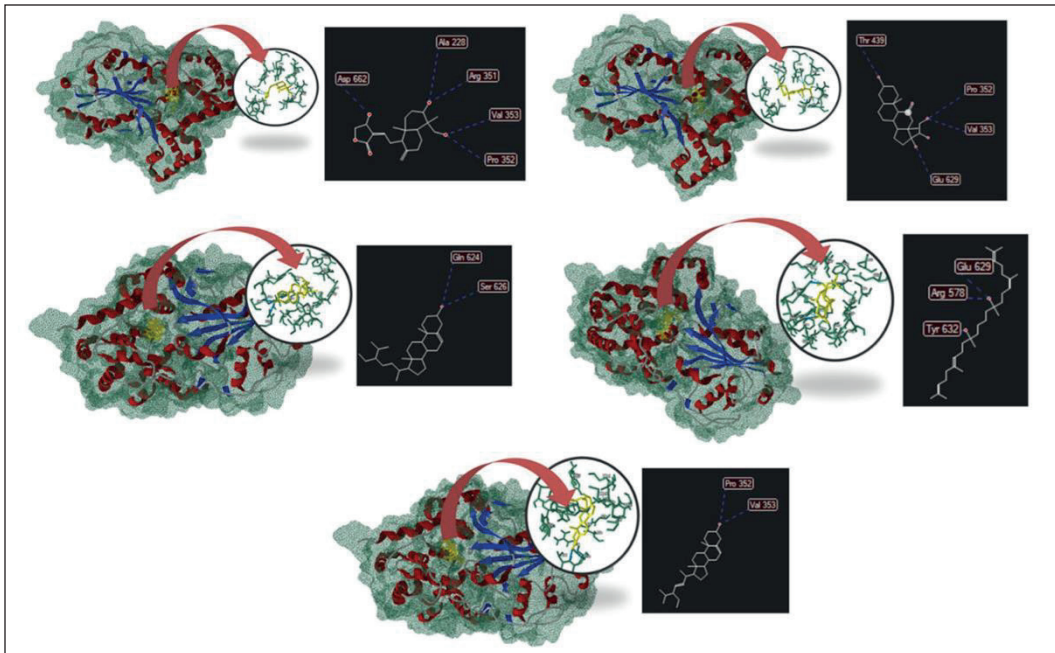


Figure 9. Two and three-dimensional visualization of the interaction of the five selected compounds to the NLRP3 kinase protein binding site. (A) andrographolide, (B) cortolone, (C) stigmasterol, (D) PMT, and (E) gamma-sitosterol. NLRP3 = NLR family pyrin domain-containing 3; PMT = 2,6,10,15,19,23-pentamethyl-2,6,18,22-tetracosatetraen-10,15-diol.

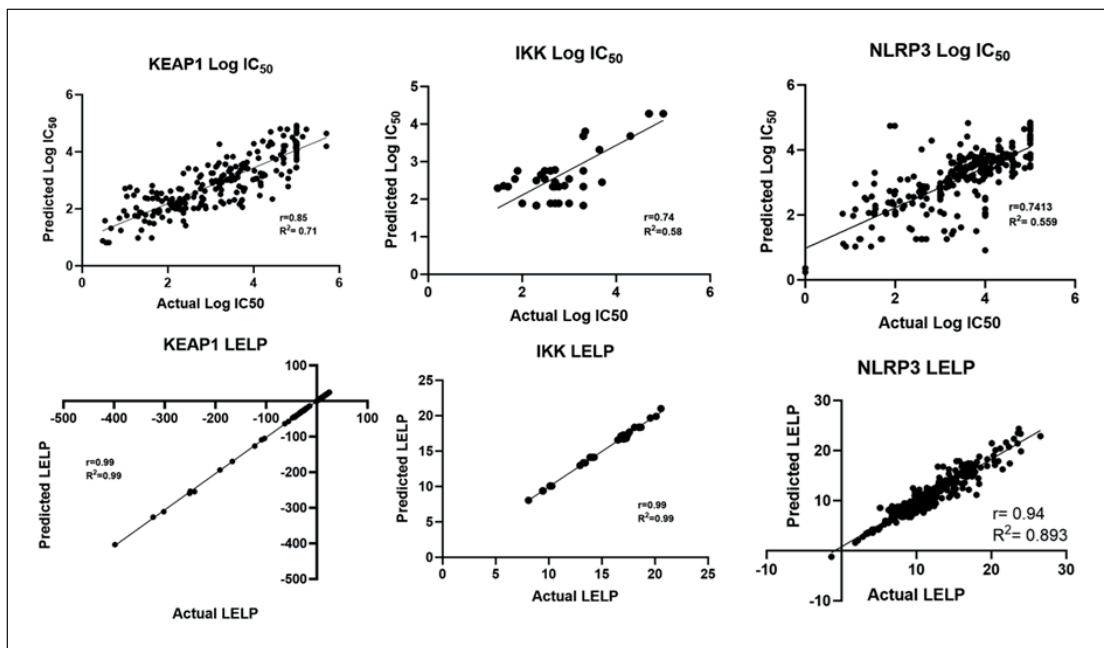


Figure 10. Validation of data training of compound present in ChEMBI database for MFP analysis prediction in Log IC_{50} and LELP. (A) Keap1 Log IC_{50} , (B) IKK Log IC_{50} , (C) NLRP3 Log IC_{50} , (D) Keap1 LELP, (E) IKK LELP, and (F) NLRP3 LELP, which showing $R^2 > 0.5$ and $r > 0.5$. IC_{50} = half maximal inhibitory concentration; IKK = inhibitor of Kappa B kinase; Keap1 = Kelch-like ECH associated protein 1; LELP = ligand efficiency lipophilicity; NLRP3 = NLR family pyrin domain-containing 3.

CYP3A4, while stigmasterol inhibits CYP2D6. The remaining compounds show no significant interactions with CYP enzymes. Regarding excretion, Andrographolide and Cortolone are P-glycoprotein substrates, whereas the other three compounds

are not, suggesting they cannot clear effectively through the liver or kidneys.

In terms of toxicity, stigmasterol and gamma-sitosterol have a high predicted acute toxicity level, with both showing an

Table 7. MFP analysis of IC50 and LELP of predominant compound against Keap1, IKK, and NLRP3.

| Compound | Keap1 | | IKK | | NLRP3 | |
|------------------|------------------------|----------|------------------------|----------|------------------------|----------|
| | pIC ₅₀ (μM) | pLELP | pIC ₅₀ (μM) | pLELP | pIC ₅₀ (μM) | pLELP |
| PMT | 0.20 (E) | 30.7 (U) | 7.27 (G) | 30.8 (U) | 2.36 (G) | 30.0 (U) |
| Cortolone | 1.52 (G) | 3.4 (I) | 7.11 (G) | 3.5 (I) | 1.75 (G) | 3.4 (I) |
| Andrographolide | 4.23 (G) | 4.1 (I) | 10.0 (G) | 4.1 (I) | 1.77 (G) | 3.4 (I) |
| Gamma-sitosterol | 2.24 (G) | 19.7 (U) | 6.2 (G) | 20.4 (U) | 2.17 (G) | 19.9 (U) |
| Stigmasterol | 2.69 (G) | 20.4 (U) | 6.8 (G) | 19.7 (U) | 1.72 (G) | 19.3 (U) |

E = excellent potency; G = good potency; I = Ideal; PMT = 2,6,10,15,19,23-pentamethyl-2,6,18,22-tetracosatetraen-10,15-diol; U = unideal.

Table 8. ADMET properties of predominant compound.

| Compound | Administration | Distribution | Metabolism (CYP substrate isoform) | | | | | Excretion | Toxicity | | | | | | |
|------------------|----------------|--------------|------------------------------------|------|-----|-----|-----|---------------|--------------|----|----|----|----|------|-----|
| | GI-A | BBB-P | 1A2 | 2C19 | 2C9 | 2D6 | 3A4 | Pgp substrate | AT (mg/kgbw) | HT | NT | CT | MT | CarT | CyT |
| PMT | Low | No | Yes | No | No | No | Yes | No | 5,000 | I | I | I | I | I | I |
| Cortolone | High | No | No | No | No | No | No | Yes | 3,000 | I | I | A | I | I | I |
| Andrographolide | High | No | No | No | No | No | No | Yes | 1,890 | I | I | A | I | I | I |
| Stigmasterol | Low | No | No | No | No | Yes | No | No | 890 | I | I | I | I | I | I |
| Gamma-sitosterol | Low | No | No | No | No | No | No | No | 890 | I | I | I | I | I | I |

A = active; AT = acute toxicity; BBB-P = blood brain barrier permeability; CarT = carcinogenicity; CT = cardiotoxicity; CYP = cytochrome P450; Cyt = cytotoxicity; GI-A = gastrointestinal absorption; HT = hepatotoxicity; I = inactive; MT = mutagenicity; NT = neurotoxicity; Pgp = P-glycoprotein; PMT = 2,6,10,15,19,23-pentamethyl-2,6,18,22-tetracosatetraen-10,15-diol.

LD₅₀ of 890 mg/kgbw. Andrographolide has an LD₅₀ of 1,890 mg/kgbw, Cortolone 3,000 mg/kgbw, and PMT 5,000 mg/kgbw. Most compounds are not expected to cause hepatotoxicity, nephrotoxicity, cardiotoxicity, mutagenicity, carcinogenicity, or cytotoxicity, except for Andrographolide and Cortolone, which show predicted cardiotoxic activity.

DISCUSSION

Our current research demonstrates that Ang-II at 1 μM induces hypertrophy in H9c2 cells, characterized by increased CSA and elevated BNP and AT1R mRNA levels. This hypertrophic response was accompanied by activation of intracellular proinflammatory pathways, evidenced by upregulated mRNA expression of NLRP3, NF-κB, and IL-1β. Concurrently, we observed a redox imbalance with elevated ROS and H₂O₂ levels and reduced mRNA expression of Nrf2 and SOD1. Treatment of Ang-II-exposed H9c2 cells with APE reduced CSA and hypertrophic marker expression, effectively suppressing the NLRP3/NF-κB/IL-1β pathway. Additionally, APE restored redox balance by upregulating Nrf2 and SOD1 mRNA expression comparable to Irbesartan, which also exhibited anticardiac hypertrophy, antioxidant, and anti-inflammation activity in similar pathways [57,58]. To the best of our knowledge, this study is the first to report the efficacy of APE in mitigating cardiac hypertrophy via the NLRP3/NF-κB/IL-1β pathway and alleviating oxidative stress through Nrf2 signaling.

Previous studies using cardiac hypertrophy and doxorubicin cardiac injury models emphasize that whole *A. paniculata* extract mitigates cardiac disease by suppressing the

proinflammation and oxidative stress pathways [23,24,40,59]. Furthermore, our previous studies confirmed that dried APE containing 8.98% Andrographolide reduces serum BNP and cardiac troponin I levels *in vivo* doxorubicin rat models [41]. We consider APE's abilities to inhibit hypertrophy progression of H9c2 through modulating Nrf2/NF-κB/NLRP3 in this research as part of proving its mechanism to modulate proinflammation and oxidative stress pathways.

A. paniculata contains various bioactive compounds such as terpenoids, flavonoids, alkaloids, steroids, tannins, and saponins. The presence of these compounds can vary based on the plant part [60], geographic location [61], extraction solvents [62], and methods used [60]. Our analysis of APE identified terpenoids, flavonoids, steroids, and tannins. However, alkaloids, saponins, and glycosides were not detected, which differs from previous studies that suggest alkaloid, saponin, and glycoside presence [62]. Notably, Andrographolide, a diterpene lactone, was the second most abundant compound (12.28% by GC-MS analysis). Despite the abundant terpenoid content in this extract, limitations of GC-MS in detecting high molecular weight and highly polar compounds prevented the identification of other terpenoid forms, such as neoandrographolide, 14-deoxyandrographolide, and andrographanin [9,60]. Future studies may benefit from using alternative methods, such as nuclear magnetic resonance spectroscopy or high-performance liquid chromatography, particularly in identifying new compounds like PMT, to validate these findings.

Inflammation and oxidative stress are closely linked to cardiac remodeling [32,35]. Chronic ROS elevation can initiate inflammation in HF, exacerbated by neurohumoral

activation, such as Ang-II stimulation of cardiomyocytes [26]. Ang-II activates NF- κ B, a pivotal mediator that senses increased intracellular ROS production and primes the NLRP3 inflammasome signaling pathway, resulting in IL-1 β mRNA expression [35]. In our Ang-II-treated H9c2 cells, activation of NF- κ B (p50), NLRP3, and IL-1 β was observed, consistent with prior research. Under normal conditions, Nrf2 responds to ROS-induced cellular stress by dissociating from Keap1, binding to antioxidant response elements (AREs), and upregulating intrinsic antioxidant mRNA transcription. However, NF- κ B binding to the κ B site can inhibit Nrf2-ARE signaling, further downregulating antioxidant mRNA transcription [36]. Additionally, exceeding the capacity of this signaling pathway to counteract redox imbalance may help downregulate Nrf2 and SOD1 presented in our Ang-II-treated H9c2 cells.

In our study, APE effectively attenuated Ang-II-induced H9c2 cell hypertrophy by suppressing proinflammatory signaling through NF- κ B/NLRP3/IL-1 β . Nrf2 can suppress the NLRP3 signaling by reducing ROS and inducing anti-inflammation protein, NADPH Quinone Dehydrogenase-1 that directly inhibits NLRP3 priming [33,34], which becomes one probable reason caused by the increase of Nrf2 mRNA expression and decrease of NLRP3 mRNA expression. In this situation, NF- κ B downregulation is also involved, as NLRP3 activation is initiated by priming signaling from NF- κ B. Previous studies have shown that APE increases Nrf2/ARE signaling [63,64] and reduces NF- κ B/NLRP3/IL-1 β [65] signaling in non-cardiovascular disease models. Our study is the first to demonstrate enhanced Nrf2/ARE signaling in cardiac hypertrophy using APE. Although we did not directly compare APE with isolated Andrographolide in terms of antihypertrophic [66,67], antioxidant [16,39,68], and anti-inflammatory [69] effects, previous research suggests that whole extract formulations often exhibit superior therapeutic effects, possibly due to synergistic interactions among multiple compounds. The above phenomenon may explain the potential synergistic effects of various compounds in APE, enhancing its pharmacological efficacy beyond that of isolated constituents [70,71].

To predict the mechanism and potential synergistic effects of compounds identified in APE in modulating the NF- κ B/NLRP3/IL-1 β axis and Nrf2/ARE, we next conducted *in silico* analyses. Our findings demonstrate that the entire compound mixture, particularly the five most abundant compounds—Gamma-sitosterol, Andrographolide, Cortolone, Stigmasterol, and PMT—spontaneously interact with the binding sites of IKK, NLRP3, and Keap1, exhibiting significant bioactivity as indicated by SkelSpheres molecule identifier. Notably, these compounds form strong hydrogen bonds with each protein they dock with. PMT had the most negative binding energy in molecular docking. PMT also exhibits hydrogen bond interactions like native ligands in Keap1 through Arg415 and Ser602 and NLRP3 through Arg578. The other four predominant compounds, which show higher binding energies than PMT, interact differently with the binding sites, similar to native ligands. This research is the first documented report on PMT's potential to modulate NLRP3, NF- κ B, and Nrf2 signaling pathways through *in silico* analysis.

Andrographolide and Cortolone can bind spontaneously to Keap1, IKK, and NLRP3. Even though Andrographolide exhibits different hydrogen bond interactions with IKK and Keap1, it forms five hydrogen bonds like native ligands with the NLRP3 NACHT domain, suggesting that Andrographolide, in nature, may interact spontaneously with NLRP3. Previous *in vivo* studies confirm Andrographolide's inhibition of NLRP3 inflammasome signaling and its anti-inflammatory properties by suppressing NF- κ B activation [72–74].

Additionally, Cortolone, Stigmasterol, and gamma-sitosterol are phytosterols, plant-derived steroids. Preclinical studies frequently report that dietary phytosterols exert anti-inflammatory and antioxidant effects. In our *in silico* models, these compounds demonstrate spontaneous binding and predict significant bioactivity. For example, β -sitosterol, a derivative of gamma-sitosterol, modulates the PPAR γ /NF- κ B signaling pathway in myocardial ischemia/reperfusion injury. Studies also indicate that phytosterols activate several antioxidant enzymes, including catalase (CAT), SOD, glutathione, and glutathione Peroxidase [75].

Drug discovery involves comprehensive analysis, encompassing factors such as candidates' physicochemical properties. Optimization extends beyond bioactivity to include pharmacokinetic properties, which are crucial for optimizing dosing strategies and identifying toxicity risks, particularly in clinical scenarios like HF [52]. Different compounds exhibit varying pharmacokinetic properties from absorption to excretion, predicted using computational tools such as SwissADME and Prottox. MFP analysis, including LELP, guides the selection of lead compounds based on potency (IC₅₀), physicochemical properties (lipophilicity, CLogP), and ADMET profile. Our findings highlight Andrographolide and Cortolone as drug-like candidates with favorable ADMET and LELP properties, despite predictions of potential cardiotoxicity. However, our findings did not directly compare the potency between APE and lead compounds in inhibiting hypertrophy. These results mainly suggest that the most five common compound showing good binding activity, as it present negative results of MolDock Score, but Andrographolide and Cortolone, even they did not become the most compound to have negative binding energy, the possessed good pIC₅₀ and LELP. Regarding the similarity of binding mechanism. Despite the facts that previous study much discuss on how Andrographolide promotes NF- κ B inhibition, somehow, our *in silico* studies did not reflect that as Andrographolide bind IKK with different site of hydrogen bond. Furthermore, it is interesting to see that andrographolide interact in the same binding site with native ligand of NLRP3 on Arg351. This might becoming a clue that Andrographolide interact directly with NLRP3 as it also possessed antiinflammation effect, which should be proven especially using enzyme-assay test.

Among all compounds detected, Andrographolide is the most suitable drug candidate that warrants being tested in clinical settings, as a lot of evidence from preclinical research has suggested it promotes anticardiac hypertrophy [39,66,67,76–79], has known pharmacokinetic [15], and drug-herbal interaction profile in previous studies [80]. In our *in silico* studies, Andrographolide showed good bioactivity to enhance

Nrf2 proteins and inhibit the NF- κ B and NLRP3 signaling with ideal LELP and ADMET properties. Cortolone also shows a similar feature in our study, even though its utility has not been yet explicitly discussed in many previous studies. In addition, despite the remaining compounds showing unfavorable physiochemical aspects of being a drug candidate, their use as an HF drug candidate is also potentially modified using certain strategies, especially PMT, a novel compound in this study. Drugs with high molecular weight and low absorption could potentiate their oral bioavailability by chemical modification or specific absorption enhancers using nanoparticle technology [81,82].

CONCLUSION

In conclusion, our study reveals that APE effectively inhibits hypertrophy in Ang-II-treated H9c2 cells by reducing inflammatory responses and restoring redox balance through the Nrf2/NLRP3/NF- κ B signaling pathways. Ang-II exposure led to increased CSA, elevated BNP and AT1R mRNA levels, and activation of proinflammatory markers, accompanied by oxidative stress indicated by elevated ROS and decreased Nrf2 and SOD1 mRNA expression. APE treatment mitigated these effects in a way comparable to Irbesartan, demonstrating its unique ability to suppress the inflammatory pathway while enhancing antioxidant gene expression. It should be noted that successive solvation might give better results as it aims to find a more specific fraction of this extract, which will be planned in future studies.

Notably, entire five compounds, gamma-sitosterol, andrographolide, cortolone, stigmasterol, and PMT, were found to have good predicted molecular binding and bioactivity against the Nrf2/NLRP3/NF- κ B signaling pathway to alleviate hypertrophy. Furthermore, among those five compounds, Andrographolide and Cortolone found in this APE become suitable drug candidate supported by *in silico* analyses which highlight their ideal interactions and bioactivity with key signaling proteins, added with good pharmacokinetic profiles. These results warrant further *in vivo* validation, such as enzyme assay studies, and exploring further therapeutic potential compounds found in this extract before further translating to the clinical scenario.

AUTHOR CONTRIBUTIONS

All authors made substantial contributions to conception and design, acquisition of data, or analysis and interpretation of data; took part in drafting the article or revising it critically for important intellectual content; agreed to submit to the current journal; gave final approval of the version to be published; and agree to be accountable for all aspects of the work. All the authors are eligible to be an author as per the International Committee of Medical Journal Editors (ICMJE) requirements/guidelines.

ACKNOWLEDGMENT

We thank Mrs. Annisa, Wita, and Ajeng for providing technical assistance and PT Konimex Indonesia for affording the APE. We also thank Mas Rizky Anggun Adipurna Syamsunarno, MD, PhD, from UNPAD for gifting the H9c2

cells, Prof. Septelia Inawati and Sherin Saheera, MD, P.hD that has give significant contributions in research idea and technical conception, and Oluebebe Eziefule Magnificent for proofreading and correcting our manuscripts.

FINANCIAL SUPPORT

The entire research was supported by the PUTI Q2 2024 Grant from Universitas Indonesia, with a number NKB-658/UN2.RST/HKP.05.00/2024.

CONFLICTS OF INTEREST

The authors report no financial or any other conflicts of interest in this work.

DATA AVAILABILITY

The mass-spectral, original *in silico* data and full histology image are available in Supplementary Materials. Further inquiries of other *in vitro* data can be achieved with clear reason by directly contacting the corresponding author.

ETHICAL APPROVALS

This study does not involve experiments on animals or human subjects.

DATA AVAILABILITY

All data generated and analyzed are included in this research article.

PUBLISHER'S NOTE

All claims expressed in this article are solely those of the authors and do not necessarily represent those of the publisher, the editors and the reviewers. This journal remains neutral with regard to jurisdictional claims in published institutional affiliation.

USE OF ARTIFICIAL INTELLIGENCE (AI)-ASSISTED TECHNOLOGY

The authors declares that they have not used artificial intelligence (AI)-tools for writing and editing of the manuscript, and no images were manipulated using AI.

REFERENCES

1. Savarese G, Becher PM, Lund LH, Seferovic P, Rosano GMC, Coats AJS. Global burden of heart failure: a comprehensive and updated review of epidemiology. *Cardiovasc Res.* 2023;118(17):3272–87. doi: <https://doi.org/10.1093/cvr/cvac013>
2. Lam CSP. Heart failure in Southeast Asia: facts and numbers. *ESC Heart Fail.* 2015;2(2):46–9. doi: <https://doi.org/10.1002/ehf2.12036>
3. McDonagh TA, Metra M, Adamo M, Baumbach A, Böhm M, Burri H, *et al.* 2021 ESC guidelines for the diagnosis and treatment of acute and chronic heart failure. *Eur Heart J.* 2021;42(36):3599–726. doi: <https://doi.org/10.1093/eurheartj/ehab670>
4. Hu Y, Liang L, Liu S, Kung JY, Banh HL. Angiotensin-converting enzyme inhibitor induced cough compared with placebo, and other antihypertensives: a systematic review, and network meta-analysis. *J Clin Hypertens (Greenwich).* 2023;25(8):661–88. doi: <https://doi.org/10.1111/jch.14695>
5. Fukushima S, Oishi M, Aso H, Arai K, Sasaki Y, Tochikura N, *et al.* Effects of angiotensin II receptor blockers on serum potassium level and hyperkalemia risk: retrospective single-centre analysis.

- Eur J Hosp Pharm. 2023;30(4):208–13. doi: <https://doi.org/10.1136/ejpharm-2021-002739>
6. Davin L, Marechal P, Lancellotti P, Martinez C, Pierard L, Radermecker R. Angioedema: a rare and sometimes delayed side effect of angiotensin-converting enzyme inhibitors. *Acta Cardiol.* 2019;74(4):277–81. doi: <https://doi.org/10.1080/00015385.2018.1507477>
 7. Ahmad H, Khan H, Haque S, Ahmad S, Srivastava N, Khan A. Angiotensin-converting enzyme and hypertension: a systemic analysis of various ACE inhibitors, their side effects, and bioactive peptides as a putative therapy for hypertension. *J Renin Angiotensin Aldosterone Syst.* 2023;2023:7890188. doi: <https://doi.org/10.1155/2023/7890188>
 8. Krittanawong C, Kitai T. Pharmacogenomics of angiotensin receptor/neprilysin inhibitor and its long-term side effects. *Cardiovasc Ther.* 2017;35(4):e12272. doi: <https://doi.org/10.1111/1755-5922.12272>
 9. Kumar S, Singh B, Bajpai V. *Andrographis paniculata* (Burm.f.) Nees: traditional uses, phytochemistry, pharmacological properties and quality control/quality assurance. *J Ethnopharmacol.* 2021;275:114054. doi: <https://doi.org/10.1016/j.jep.2021.114054>
 10. Widjajakusuma EC, Jonosewojo A, Hendriati L, Wijaya S, Ferawati, Surjadhana A, *et al.* Phytochemical screening and preliminary clinical trials of the aqueous extract mixture of *Andrographis paniculata* (Burm. f.) Wall. ex Nees and *Syzygium polyanthum* (Wight.) Walp leaves in metformin treated patients with type 2 diabetes. *Phytomedicine.* 2019;55:137–47. doi: <https://doi.org/10.1016/j.phymed.2018.07.002>
 11. Thi Hong Hanh T, Thi Thuy My N, Thi Cham P, Hong Quang T, Xuan Cuong N, Thu Huong T, *et al.* Diterpenoids and flavonoids from *Andrographis paniculata*. *Chem Pharm Bull (Tokyo).* 2020;68(1):96–9. doi: <https://doi.org/10.1248/cpb.c19-00662>
 12. Worakunphanich W, Thavorncharoensap M, Youngkong S, Thadanipon K, Thakkinstian A. Safety of *Andrographis paniculata*: a systematic review and meta-analysis. *Pharmacoepidemiol Drug Saf.* 2021;30(6):727–39. doi: <https://doi.org/10.1002/pds.5190>
 13. Plianrungrsi J, Kulthanaamondhita P. Comparison of *Andrographis paniculata* and chlorhexidine mouthwash on anti-plaque, anti-gingivitis and side effects. *J Dent Assoc Thai.* 2021;71(4):321–9. doi: <https://doi.org/10.14456/jdat.2021.35>
 14. Okonogi R, Thampanya V, Okonogi S. Efficacy of *Andrographis paniculata* spray in acute pharyngitis: a randomized controlled trial. *Drug Discov Ther.* 2023;17(5):340–5. doi: <https://doi.org/10.5582/ddt.2023.01053>
 15. Songvut P, Rangkadilok N, Pholphana N, Suriyo T, Panomvana D, Puranajoti P, *et al.* Comparative pharmacokinetics and safety evaluation of high dosage regimens of *Andrographis paniculata* aqueous extract after single and multiple oral administration in healthy participants. *Front Pharmacol.* 2023;14:1230401. doi: <https://doi.org/10.3389/fphar.2023.1230401>
 16. Baru Venkata R, Prasanth DSNBK, Pasala PK, Panda SP, Tatipamula VB, Mulukuri S, *et al.* Utilizing *Andrographis paniculata* leaves and roots by effective usage of the bioactive andrographolide and its nanodelivery: investigation of antikinlding and antioxidant activities through in silico and in vivo studies. *Front Nutr.* 2023;10:1185236. doi: <https://doi.org/10.3389/fnut.2023.1185236>
 17. Bosco F, Ruga S, Citraro R, Leo A, Guarnieri L, Maiuolo J, *et al.* The effects of *Andrographis paniculata* (Burm.F.) Wall. ex Nees and andrographolide on neuroinflammation in the treatment of neurodegenerative diseases. *Nutrients.* 2023;15(15):3428. doi: <https://doi.org/10.3390/nu15153428>
 18. Sule A, Ahmed QU, Samah OA, Omar MN. Bacteriostatic and bactericidal activities of *Andrographis paniculata* extracts on skin disease causing pathogenic bacteria. *J Med Plant Res.* 2011;5(1):7–14. doi: <https://doi.org/10.5897/JMPR.9000288>
 19. Malik Z, Parveen R, Parveen B, Zahiruddin S, Khan MA, Khan A, *et al.* Anticancer potential of andrographolide from *Andrographis paniculata* (Burm.f.) Nees and its mechanisms of action. *J Ethnopharmacol.* 2021;272:113936. doi: <https://doi.org/10.1016/j.jep.2021.113936>
 20. Sa-Ngiamsumtorn K, Suksatu A, Pewkliang Y, Thongsri P, Kanjanasirirat P, Manopwisedjaroen S, *et al.* Anti-SARS-CoV-2 activity of *Andrographis paniculata* extract and its major component Andrographolide in human lung epithelial cells and cytotoxicity evaluation in major organ cell representatives. *J Nat Prod.* 2021;84(4):1261–70. doi: <https://doi.org/10.1021/acs.jnatprod.0c01324>
 21. Majumdar M, Singh V, Misra TK, Roy DN. In silico studies on structural inhibition of SARS-CoV-2 main protease Mpro by major secondary metabolites of *Andrographis paniculata* and *Cinchona officinalis*. *Biologia (Bratisl).* 2022;77(5):1373–89. doi: <https://doi.org/10.1007/s11756-022-01012-y>
 22. Ischak NI, Botutihe DN. Preliminary study of clinical antidiabetic activity of salam leaves (*Eugenia Polyantha*) and sambiloto leaves (*Andrographis paniculata*) in type 2 diabetic patients. *IOP Conf Ser Earth Environ Sci.* 2020;589(2020):010234. doi: <https://doi.org/10.1088/1755-1315/589/1/010234>
 23. Hsieh YL, Shibu MA, Lii CK, Viswanadha VP, Lin YL, Lai CH, *et al.* *Andrographis paniculata* extract attenuates pathological cardiac hypertrophy and apoptosis in high-fat diet fed mice. *J Ethnopharmacol.* 2016;192:170–7. doi: <https://doi.org/10.1016/j.jep.2016.07.018>
 24. Ojha SK, Bharti S, Joshi S, Kumari S, Arya DS. Protective effect of hydroalcoholic extract of *Andrographis paniculata* on ischaemia-reperfusion induced myocardial injury in rats. *Indian J Med Res.* 2012;135(3):414–21.
 25. Guo ZL, Zhao HY, Zheng XH. An experimental study of the mechanism of *andrographis paniculata* nees (APN) in alleviating the Ca(2+)-overloading in the process of myocardial ischemic reperfusion. *J Tongji Med Univ.* 1995;15(4):205–8. doi: <https://doi.org/10.1007/BF02887945>
 26. Schwinger RHG. Pathophysiology of heart failure. *Cardiovasc Diagn Ther.* 2021;11(1):263–76. doi: <https://doi.org/10.21037/cdt-20-302>
 27. Siao WZ, Chen YH, Tsai CF, Lee CM, Jong GP. Diabetes mellitus and heart failure. *J Pers Med.* 2022;12(10):1698. doi: <https://doi.org/10.3390/jpm12101698>
 28. Oh GC, Cho HJ. Blood pressure and heart failure. *Clin Hypertens.* 2020;26:1. doi: <https://doi.org/10.1186/s40885-019-0132-x>
 29. Nagueh S. Heart failure with preserved ejection fraction: insights into diagnosis and pathophysiology. *Cardiovasc Res.* 2021;117(4):999–1014. doi: <https://doi.org/10.1093/cvr/cvaa228>
 30. Melaku L, Desalegn T. Molecular mediators, characterization of signaling pathways with descriptions of cellular distinctions in pathophysiology of cardiac hypertrophy and molecular changes underlying a transition to heart failure. *Int J Health Allied Sci.* 2019;8:1. doi: https://doi.org/10.4103/ijhas.IJHAS_104_17
 31. van der Pol A, van Gilst WH, Voors AA, van der Meer P. Treating oxidative stress in heart failure: past, present and future. *Eur J Heart Fail.* 2019;21(4):425–35. doi: <https://doi.org/10.1002/ejhf.1320>
 32. Van Linthout S, Tschöpe C. Inflammation – cause or consequence of heart failure or both? *Curr Heart Fail Rep.* 2017;14(4):251–65. doi: <https://doi.org/10.1007/s11897-017-0337-9>
 33. Yan R, Sun Y, Yang Y, Zhang R, Jiang Y, Meng Y. Mitochondria and NLRP3 inflammasome in cardiac hypertrophy. *Mol Cell Biochem.* 2024;479(7):1571–82. doi: <https://doi.org/10.1007/s11010-023-04812-1>
 34. Pinar AA, Scott TE, Huuskes BM, Tapia Cáceres FE, Kemp-Harper BK, Samuel CS. Targeting the NLRP3 inflammasome to treat cardiovascular fibrosis. *Pharmacol Ther.* 2020;209:107511. doi: <https://doi.org/10.1016/j.pharmthera.2020.107511>
 35. Lim S, Lee ME, Jeong J, Lee J, Cho S, Seo M, *et al.* sRAGE attenuates angiotensin II-induced cardiomyocyte hypertrophy by inhibiting RAGE-NFκB-NLRP3 activation. *Inflamm Res.* 2018;67:691–701.

36. Ahmed SMU, Luo L, Namani A, Wang XJ, Tang X. Nrf2 signaling pathway: pivotal roles in inflammation. *Biochim Biophys Acta Mol Basis Dis.* 2017;1863(2):585–97. doi: <https://doi.org/10.1016/j.bbadis.2016.11.005>
37. Satta S, Mahmoud AM, Wilkinson FL, Yvonne Alexander M, White SJ. The role of Nrf2 in cardiovascular function and disease. *Oxid Med Cell Longev.* 2017;2017:9237263. doi: <https://doi.org/10.1155/2017/9237263>
38. Eziefule OM, Arozal W, Wanandi SI, Dewi S, Nafrialdi, Saraswati M, *et al.* *Andrographis paniculata*: a potential supplementary therapy for cardiovascular diseases - A systematic review of its effects and molecular actions. *J Pharm Pharmacogn Res.* 2024;12(3):488–513. doi: https://doi.org/10.56499/jppres23.1841_12.3.487
39. Xie SY, Deng W, Chen JJ, Wu QQ, Li HJ, Wang J, *et al.* *Andrographolide* protects against adverse cardiac remodeling after myocardial infarction through enhancing Nrf2 signaling pathway. *Int J Biol Sci.* 2020;16:12–26. doi: <https://doi.org/10.7150/ijbs.37269>
40. Eziefule OM, Arozal W, Wanandi SI, Louisa M, Wuyung PE, Dewi S, *et al.* *Andrographis paniculata* ethanolic extract improved doxorubicin-induced cardiac inflammation, alterations in liver function parameters and anemia. *Mol Cell Biomed Sci.* 2024;8(2):117. doi: <https://doi.org/10.21705/mcbs.v8i2.444>
41. Arozal W, Wanandi SI, Louisa M, Wuyung PE, Noviana D, Eziefule OM, *et al.* Evaluating the acute toxicity and in vivo protective effect of standardized *Andrographis paniculata* extract against doxorubicin-induced cardiotoxicity in sprague-dawley rats. *Trop J Nat Prod Res.* 2024;8:7134–41. doi: <https://doi.org/10.26538/tjnpr/v8i5.13>
42. Han W, Ward JL, Kong Y, Li X. Editorial: targeted and untargeted metabolomics for the evaluation of plant metabolites in response to the environment. *Front Plant Sci.* 2023;14:1167513. doi: <https://doi.org/10.3389/fpls.2023.1167513>
43. Chang CC, Cheng HC, Chou WC, Huang YT, Hsieh PL, Chu PM, *et al.* Sesamin suppresses angiotensin-II-enhanced oxidative stress and hypertrophic markers in H9c2 cells. *Environ Toxicol.* 2023;38(9):2165–72. doi: <https://doi.org/10.1002/tox.23853>
44. Ren S, Wang Y, Zhang Y, Yan P, Xiao D, Zhao Y, *et al.* Paeoniflorin alleviates AngII-induced cardiac hypertrophy in H9c2 cells by regulating oxidative stress and Nrf2 signaling pathway. *Biomed Pharmacother.* 2023;165:115253. doi: <https://doi.org/10.1016/j.biopha.2023.115253>
45. Yang Y, Xie Y, Zhao X, Qi M, Liu X. Pogostone alleviates angiotensin II-induced cardiomyocyte hypertrophy in H9c2 cells through MAPK and Nrf2 pathway. *Trop J Pharm Res.* 2023;22(7):1373–8. doi: <https://doi.org/10.4314/tjpr.v22i7.3>
46. Watkins SJ, Borthwick GM, Arthur HM. The H9c2 cell line and primary neonatal cardiomyocyte cells show similar hypertrophic responses in vitro. *In Vitro Cell Dev Biol Anim.* 2011;47(2):125–31. doi: <https://doi.org/10.1007/s11626-010-9368-1>
47. Fadhillah MR, Arozal W, Wibowo H. Optimizing cell culture strategy for H9c2 cardiomyoblast: a lesson learned for building cardiovascular disease model. 2024;5:67–75. doi: <https://doi.org/10.20885/EKSAKTA.vol5.iss1.art8>
48. Indrayanto G, Putra GS, Suhud F. Validation of in-vitro bioassay methods: application in herbal drug research. *Profiles Drug Subst Excip Relat Methodol.* 2021;46:273–307. doi: <https://doi.org/10.1016/bs.podrm.2020.07.005>
49. Atale N, Mishra CB, Kohli S, Mongre RK, Prakash A, Kumari S, *et al.* Anti-inflammatory effects of *S. cumini* seed extract on gelatinase-B (MMP-9) regulation against hyperglycemic cardiomyocyte stress. *Oxid Med Cell Longev.* 2021;2021:8839479. doi: <https://doi.org/10.1155/2021/8839479>
50. Atale N, Chakraborty M, Mohanty S, Bhattacharya S, Nigam D, Sharma M, *et al.* Cardioprotective role of *Syzygium cumini* against glucose-induced oxidative stress in H9C2 cardiac myocytes. *Cardiovasc Toxicol.* 2013;13(3):278–89. doi: <https://doi.org/10.1007/s12012-013-9207-1>
51. Dwira S, Tedjo A, Dharmawan MA, Erlina L, Fadillah F. Differentially expressed genes, and molecular docking and dynamic analysis revealing the potential of compounds in zingiber officinale roscoe as inhibitors of TP53-regulating kinase (TP53RK) that influence the p53 signaling pathway related to apoptosis and cell cycle. *Trop J Nat Prod Res.* 2024;8(8):8007–13. doi: <https://doi.org/10.26538/tjnpr/v8i8.12>
52. Hopkins AL, Keserü GM, Leeson PD, Rees DC, Reynolds CH. The role of ligand efficiency metrics in drug discovery. *Nat Rev Drug Discov.* 2014;13:105–21. doi: <https://doi.org/10.1038/nrd4163>
53. Alexander DLJ, Tropsha A, Winkler DA. Beware of R2: simple, unambiguous assessment of the prediction accuracy of QSAR and QSPR models. *J Chem Inf Model.* 2015;55(7):1316–22. doi: <https://doi.org/10.1021/acs.jcim.5b00206>
54. Catalani V, Botha M, Corkery JM, Guirguis A, Vento A, Scherbaum N, *et al.* The psychonauts' benzodiazepines; quantitative structure-activity relationship (Qsar) analysis and docking prediction of their biological activity. *Pharmaceuticals (Basel).* 2021;14(8):720. doi: <https://doi.org/10.3390/ph14080720>
55. Degoe DA, Chen HJ, Cox PB, Wendt MD. Beyond the rule of 5: lessons learned from AbbVie's drugs and compound collection. *J Med Chem.* 2018;61(7):2636–51. doi: <https://doi.org/10.1021/acs.jmedchem.7b00717>
56. Duangrat R, Parichatikanond W, Morales NP, Pinthong D, Mangmool S. Sustained AT1R stimulation induces upregulation of growth factors in human cardiac fibroblasts via Gαq/TGF-β/ERK signaling that influences myocyte hypertrophy. *Eur J Pharmacol.* 2022;937:175384. doi: <https://doi.org/10.1016/j.ejphar.2022.175384>
57. Li Y, Long W, Zhang H, Zhao M, Gao M, Guo W, *et al.* Irbesartan ameliorates diabetic nephropathy by activating the Nrf2/Keap1 pathway and suppressing NLRP3 inflammasomes in vivo and in vitro. *Int Immunopharmacol.* 2024;131:111844. doi: <https://doi.org/10.1016/j.intimp.2024.111844>
58. Rong L, Sun S, Zhu F, Xu Q, Li H, Gao Q, *et al.* Effects of irbesartan on myocardial injury in diabetic rats: the role of NLRP3/ASC/Caspase-1 pathway. *J Renin Angiotensin Aldosterone Syst.* 2020;21(2):1470320320926049. doi: <https://doi.org/10.1177/1470320320926049>
59. Wang H, Yu X, Xun Z, Wu Y. Aqueous extract of *Andrographis paniculata* ameliorates cardiotoxicity induced by doxorubicin in vivo. *Int J Pharmacol.* 2022;18:466–74. doi: <https://doi.org/10.3923/ijp.2022.466.474>
60. Rafi M, Karomah AH, Heryanto R, Septaningsih DA, Kusuma WA, Amran MB, *et al.* Metabolite profiling of *Andrographis paniculata* leaves and stem extract using UHPLC-Orbitrap-MS/MS. *Nat Prod Res.* 2022;36(2):625–29. doi: <https://doi.org/10.1080/14786419.2020.1789637>
61. Jacob George A, John Kariyil B, Krishna D. Phytochemical evaluation of *Andrographis paniculata* L. (L.). *J Pharmacogn Phytochem.* 2018;7(4):1949–53. Available from: <https://www.phytojournal.com/archives/2018/vol7issue4/PartAG/7-4-21-908.pdf>
62. Rafi M, Devi AF, Syafitri UD, Heryanto R, Suparto IH, Amran MB, *et al.* Classification of *Andrographis paniculata* extracts by solvent extraction using HPLC fingerprint and chemometric analysis. *BMC Res Notes.* 2020;13(1):56. doi: <https://doi.org/10.1186/s13104-020-4920-x>
63. Ma J, Zheng M, Zhang X, Lu J, Gu L. Ethanol extract of *Andrographis paniculata* alleviates aluminum-induced neurotoxicity and cognitive impairment through regulating the p62-keap1-Nrf2 pathway. *BMC Complement Med Ther.* 2023;23(1):441. doi: <https://doi.org/10.1186/s12906-023-04290-4>
64. Chen H-W, Huang Y-J, Yao H-T, Lii C-K. Induction of Nrf2-dependent antioxidation and protection against carbon tetrachloride-

- induced liver damage by *Andrographis paniculata* herba (chuān xīn lián) ethanolic extract. *J Tradit Complement Med.* 2012;2(3):211–9. doi: [https://doi.org/10.1016/s2225-4110\(16\)30102-x](https://doi.org/10.1016/s2225-4110(16)30102-x)
65. Rahmi EP, Kumolosasi E, Jalil J, Buang F, Jamal JA. Extracts of *Andrographis paniculata* (Burm.f.) Nees leaves exert anti-gout effects by lowering uric acid levels and reducing monosodium urate crystal-induced inflammation. *Front Pharmacol.* 2022;12:787125. doi: <https://doi.org/10.3389/fphar.2021.787125>
 66. Tian Q, Liu J, Chen Q, Zhang M. Andrographolide contributes to the attenuation of cardiac hypertrophy by suppressing endoplasmic reticulum stress. *Pharm Biol.* 2023;61(1):61–8. doi: <https://doi.org/10.1080/13880209.2022.2157021>
 67. Wu QQ, Ni J, Zhang N, Liao HH, Tang QZ, Deng W. Andrographolide protects against aortic banding-induced experimental cardiac hypertrophy by inhibiting MAPKs signaling. *Front Pharmacol.* 2017;8:808. doi: <https://doi.org/10.3389/fphar.2017.00808>
 68. Otong ES, Makena W, Solomon AY, Bazabang SA, Aminu A, Henry R. *Andrographis paniculata* protects against brain hippocampus and cerebellum from mercury chloride induced damage by attenuating oxidative stress. *Environ Anal Health Toxicol.* 2022;37(4):e2022027-0. doi: <https://doi.org/10.5620/eah.2022027>
 69. Li X, Yuan W, Wu J, Zhen J, Sun Q, Yu M. Andrographolide, a natural anti-inflammatory agent: an update. *Front Pharmacol.* 2022;13:920435. doi: <https://doi.org/10.3389/fphar.2022.920435>
 70. Chen CC, Lii CK, Lin YH, Shie PH, Yang YC, Huang CS, *et al.* *Andrographis paniculata* improves insulin resistance in high-fat diet-induced obese mice and TNF α -treated 3T3-L1 adipocytes. *Am J Chin Med.* 2020;48(5):1073–90. doi: <https://doi.org/10.1142/S0192415X20500524>
 71. Adiguna SP, Panggabean JA, Swasono RT, Rahmawati SI, Izzati F, Bayu A, *et al.* Evaluations of andrographolide-rich fractions of *Andrographis paniculata* with enhanced potential antioxidant, anticancer, antihypertensive, and anti-inflammatory activities. *Plants.* 2023;12(6):1220. doi: <https://doi.org/10.3390/plants12061220>
 72. Yu Y, Miao TW, Xiao W, Mao B, Du LY, Wang Y, *et al.* Andrographolide attenuates NLRP3 inflammasome activation and airway inflammation in exacerbation of chronic obstructive pulmonary disease. *Drug Des Devel Ther.* 2024;18:1755–70. doi: <https://doi.org/10.2147/DDDT.S445788>
 73. Li J, Yang X, Yang P, Xu K, Peng X, Cai W, *et al.* Andrographolide alleviates bleomycin-induced NLRP3 inflammasome activation and epithelial-mesenchymal transition in lung epithelial cells by suppressing AKT/mTOR signaling pathway. *Ann Transl Med.* 2021;9(9):764. doi: <https://doi.org/10.21037/atm-20-7973>
 74. Peng S, Gao J, Liu W, Jiang C, Yang X, Sun Y, *et al.* Andrographolide ameliorates OVA-induced lung injury in mice by suppressing ROS-mediated NF- κ B signaling and NLRP3 inflammasome activation. *Oncotarget.* 2016;7(49):80262–74. doi: <https://doi.org/10.18632/oncotarget.12918>
 75. El Omari N, Bakrim S, Khalid A, Abdalla AN, Iesa MAM, El Kadri K, *et al.* Unveiling the molecular mechanisms: dietary phytosterols as guardians against cardiovascular diseases. *Nat Prod Bioprospect.* 2024;14(1):27. doi: <https://doi.org/10.1007/s13659-024-00451-176>
 76. Sun YT, Xu H, Tan B, Yi Q, Liu HW, Tian J, *et al.* Andrographolide-treated bone marrow mesenchymal stem cells-derived conditioned medium protects cardiomyocytes from injury by metabolic remodeling. *Mol Biol Rep.* 2023;50(3):2651–62. doi: <https://doi.org/10.1007/s11033-023-08250-6>
 77. Zhong XM, Zeng XL, Li B, Li X, Huang ZH, Zeng J. Andrographolide inhibit isoproterenol-induced myocardial hypertrophy in rats by reducing the excessive activation of autophagy. *Eur J Pharmacol.* 2021;906:174194. doi: <https://doi.org/10.1016/j.ejphar.2021.174194>
 78. Liang E, Liu X, Du Z, Yang R, Zhao Y. Andrographolide ameliorates diabetic cardiomyopathy in mice by blockage of oxidative damage and NF- κ B-mediated inflammation. *Oxid Med Cell Longev.* 2018;2018:9086747. doi: <https://doi.org/10.1155/2018/9086747>
 79. Lin KH, Asokan SM, Kuo WW, Hsieh YL, Lii CK, Viswanadha V, *et al.* Andrographolide mitigates cardiac apoptosis to provide cardioprotection in high-fat-diet-induced obese mice. *Environ Toxicol.* 2020;35(6):707–13. doi: <https://doi.org/10.1002/tox.22906>
 80. Sundhani E, Lukitaningsih E, Nurrochmad A, Nugroho AE. Potential pharmacokinetic and pharmacodynamic herb-drug interactions of *Andrographis paniculata* (Burm. f.) and andrographolide: a systematic review. *J HerbMed Pharmacol.* 2022;11:154–65. doi: <https://doi.org/10.34172/jhp.2022.20>
 81. Asano D, Takakusa H, Nakai D. Oral absorption of middle-to-large molecules and its improvement, with a focus on new modality drugs. *Pharmaceutics.* 2023;16(1):47. doi: <https://doi.org/10.3390/pharmaceutics16010047>
 82. Liu P, Chen G, Zhang J. A review of liposomes as a drug delivery system: current status of approved products, regulatory environments, and future perspectives. *Molecules.* 2022;27(4):1372. doi: <https://doi.org/10.3390/molecules27041372>

How to cite this article:

Fadhillah MR, Wibowo H, Bustami A, Sukmawati D, Tedjo A, Khatimah NG, Shimizu I, Arozal W. Investigation of anti-cardiac hypertrophy effects of *Andrographis paniculata* ethanolic extract by modulating proinflammation and oxidative stress via Nrf2/NF- κ B/NLRP3 signaling pathway: *In silico* and *in vitro* approaches *J Appl Pharm Sci.* 2025;15(06):277–294. DOI: 10.7324/JAPS.2025.226923

SUPPLEMENTARY MATERIAL:

The supplementary material can be accessed at the journal's website:
Link here [<http://japsonline.com/Suppl-material-10.7324JAPS.2025.226923.rar>].